



# Trichoplusia ni Kinesin-1 Associates with Autographa californica Multiple Nucleopolyhedrovirus Nucleocapsid Proteins and Is Required for Production of Budded Virus

Siddhartha Biswas, a Gary W. Blissard, David A. Theilmanna,c

Faculty of Land and Food Systems, University of British Columbia, Vancouver, British Columbia, Canada<sup>a</sup>; Boyce Thompson Institute at Cornell University, Ithaca, New York, USA<sup>b</sup>; Summerland Research and Development Centre, AAFC, Summerland, British Columbia, Canada<sup>c</sup>

#### **ABSTRACT**

The mechanism by which nucleocapsids of *Autographa californica* multiple nucleopolyhedrovirus (AcMNPV) egress from the nucleus to the plasma membrane, leading to the formation of budded virus (BV), is not known. AC141 is a nucleocapsid-associated protein required for BV egress and has previously been shown to be associated with β-tubulin. In addition, AC141 and VP39 were previously shown by fluorescence resonance energy transfer by fluorescence lifetime imaging to interact directly with the *Drosophila melanogaster* kinesin-1 light chain (KLC) tetratricopeptide repeat (TPR) domain. These results suggested that microtubule transport systems may be involved in baculovirus nucleocapsid egress and BV formation. In this study, we investigated the role of lepidopteran microtubule transport using coimmunoprecipitation, colocalization, yeast two-hybrid, and small interfering RNA (siRNA) analyses. We show that nucleocapsid AC141 associates with the lepidopteran *Trichoplusia ni* KLC and kinesin-1 heavy chain (KHC) by coimmunoprecipitation and colocalization. Kinesin-1, AC141, and microtubules colocalized predominantly at the plasma membrane. In addition, the nucleocapsid proteins VP39, FP25, and BV/ODV-C42 were also coimmunoprecipitated with *T. ni* KLC. Direct analysis of the role of *T. ni* kinesin-1 by downregulation of KLC by siRNA resulted in a significant decrease in BV production. Nucleocapsids labeled with VP39 fused with three copies of the mCherry fluorescent protein also colocalized with microtubules. Yeast two-hybrid analysis showed no evidence of a direct interaction between kinesin-1 and AC141 or VP39, suggesting that either other nucleocapsid proteins or adaptor proteins may be required. These results further support the conclusion that microtubule transport is required for AcMNPV BV formation.

## **IMPORTANCE**

In two key processes of the replication cycle of the baculovirus *Autographa californica* multiple nucleopolyhedrovirus (AcMNPV), nucleocapsids are transported through the cell. These include (i) entry of budded virus (BV) into the host cell and (ii) egress and budding of nucleocapsids newly produced from the plasma membrane. Prior studies have shown that the entry of nucleocapsids involves the polymerization of actin to propel nucleocapsids to nuclear pores and entry into the nucleus. For the spread of infection, progeny viruses must rapidly exit the infected cells, but the mechanism by which AcMNPV nucleocapsids traverse the cytoplasm is unknown. In this study, we examined whether nucleocapsids interact with lepidopteran kinesin-1 motor molecules and are potentially carried as cargo on microtubules to the plasma membrane in AcMNPV-infected cells. This study indicates that microtubule transport is utilized for the production of budded virus.

"he baculovirus Autographa californica multiple nucleopolyhedrovirus (AcMNPV) is an enveloped virus containing a large double-stranded circular DNA genome of approximately 134 kbp that encodes approximately 156 proteins. During the course of AcMNPV infection, nucleocapsids assemble in the nuclei of infected cells and subsequently produce two forms of virions, budded virus (BV) and occlusion-derived virus (ODV). A BV is typically formed from a single nucleocapsid that egresses from the nucleus, traverses the cytoplasm, and obtains an envelope by budding from the plasma membrane. ODVs are formed in the nucleus when single or multiple nucleocapsids get surrounded by a membrane that is derived from the nuclear envelope (1). BV facilitates the systemic cell-to-cell spread of the infection within the host insect, whereas ODVs become incorporated into polyhedral occlusion bodies which are liberated from the nucleus when the host insect dies and disintegrates. Occlusion bodies containing ODV mediate environmental transmission of the virus between hosts (2).

Proteomic and other analyses have identified many BV pro-

teins that are required for the nucleocapsid structure, are associated with the nucleocapsid, or are envelope proteins (3). One of the nucleocapsid-associated proteins is the 261-amino-acid protein AC141 (or EXON0), which is expressed at late times postinfection (p.i.) and is required for BV production (4–6). The deletion of *ac141* reduces BV production by 99.99%, and electron micrographs have shown that in cells infected with *ac141*-knockout virus, nucleocapsids are not able to escape the nucleus (5).

Received 17 November 2015 Accepted 8 January 2016

Accepted manuscript posted online 13 January 2016

Citation Biswas S, Blissard GW, Theilmann DA. 2016. *Trichoplusia ni* kinesin-1 associates with *Autographa californica* multiple nucleopolyhedrovirus nucleocapsid proteins and is required for production of budded virus. J Virol 90:3480–3495. doi:10.1128/JVI.02912-15.

Editor: G. McFadden

Address correspondence to David A. Theilmann, david.theilmann@agr.gc.ca. Copyright © 2016, American Society for Microbiology. All Rights Reserved.

AC141 contains a RING domain, a leucine zipper domain (required for dimerization), and regions of acidic and charged amino acids (6). Immunolocalization of AC141 has also shown that, in addition to being associated with purified nucleocapsids, it is found concentrated near the inner nuclear membrane as well as the plasma membrane (5).

During the systemic infection of a host insect or in cell culture, AcMNPV BV utilizes the major envelope fusion glycoprotein GP64 for binding and entry (7, 8). After cell entry via receptormediated endocytosis, nucleocapsids induce host F-actin polymerization, which drives them toward the nucleus and nuclear pores (9–12). Upon entering the nucleus, the viral genome is released from the nucleocapsid, and this is followed by viral early transcription, DNA replication, and late transcription, all of which are required for the production of new progeny nucleocapsids. Nucleocapsids are produced in a region of the infected cell nucleus called the virogenic stroma. Data suggest that nucleocapsid transport from the stroma to the nuclear periphery requires host nuclear F actin (13-15). Nucleocapsids escape from the nucleus possibly by a budding type of process (5, 16). The nucleocapsids then traverse the cytoplasm to the viral budding sites on the plasma membrane, from which BVs are released. The mechanism by which nucleocapsids are transported through the cytoplasm to the plasma membrane is not known. More recently, it has been suggested that nucleocapsids associate with microtubules to facilitate trafficking through the cytoplasm. AcMNPV AC141, which is required for BV production, interacts with  $\beta$ -tubulin, suggesting that microtubules are involved. In support of this, the depolymerization of microtubules substantially reduces the level of BV production (17, 18). In addition, fluorescence resonance energy transfer by fluorescence lifetime imaging (FRET-FLIM) analysis has shown that both AC141 and VP39 (a major capsid protein) interact with the tetratricopeptide repeat (TPR) domain of Drosophila melanogaster kinesin-1 light chain (DmKLC) (18). The kinesin superfamily (KIF) is a class of motor proteins which are known to carry cargo like membranous organelles and other macromolecules anteriorly along microtubules (19). Kinesin-1, also known as conventional kinesin, belongs to the KIF5 family and is a heterotetrameric protein comprising two kinesin-1 heavy chains (KHCs) and two KLCs. KHCs contain an N-terminal motor domain which drives movement along microtubules by hydrolyzing ATP. Adjacent to the motor domain is a coiled-coil stalk domain followed by a C-terminal globular tail domain (20). KLC is comprised of N-terminal heptad repeats and six C-terminal TPR motifs (21, 22). The heptad repeats of KLC interact with the stalk domain of KHC. The TPR motifs and the stalk/tail domain of KHC are also known to bind cargo (21, 23, 24). DNA viruses, such as African swine fever virus (ASFV), vaccinia virus, and herpes simplex virus 1 (HSV-1), are known to associate with the microtubule transport system and kinesin-1 as cargo for both cellular entry and egress (25-40).

As indicated above, prior studies indicate that microtubules and kinesin-1 are potentially required for the egress of AcMNPV BV. In the current study, we examined whether the native lepidopteran host cell kinesin-1 interacts with viral proteins and if it is required for nucleocapsid transport and BV production. We show that the nucleocapsid proteins AC141, VP39 (a major capsid protein), BV/ODV-C42, and FP25 associate with kinesin-1. The results of this study provide further evidence that kinesin-1 and

microtubule transport are required for AcMNPV nucleocapsid egress and BV production.

### **MATERIALS AND METHODS**

Cells and viruses. Trichoplusia ni BTI-Tn5B1-4 [Tn5B1]) cells were maintained in TC100 medium (Grace's insect medium [Gibco Life Technologies] supplemented with L-glutamine, 3.33 g/liter lactalbumin hydrolysate, 3.33 g/liter yeastolate, and 10% fetal bovine serum[FBS]) at 27°C. Polyclonal stably transformed cell lines were maintained in the same medium but in the presence of zeocin (250 µg/liter). Wild-type (WT) virus was AcMNPV strain E2. Virus expressing hemagglutinin (HA)-tagged AC141, which for this study we have called ac141KO-HA-AC141, has been previously described as exon0KO-HA-EXON0 (5). AcMNPV VP39 fused with three copies of the mCherry fluorescent protein (VP39-3×mCherry) was constructed by amplifying VP39-3×mCherry by PCR from the WOBCAT vector (a gift from Matthew D. Welch) (11) and placing it into the transfer vector pFAcT (4), generating pFAcT-VP39-3mCherry. pFAcT-VP39-3mCherry was used to insert VP39-3×mCherry into the polyhedrin locus of the bacmid bMON14272 by Tn7-mediated transposition, as previously described (41).

Cloning of T. ni KLC and KHC. The T. ni KHC and KLC sequences were initially determined from a transcriptome analysis of a T. ni Tnms42 cell (42). To clone KLC and KHC cDNA, total RNA was isolated from Tn5B1 cells using the TRIzol reagent (Ambion). The cDNAs of KLC and KHC were PCR amplified from total RNA by using SuperScript III reverse transcriptase (RT; Invitrogen Life Technologies), and primer pairs (Table 1) 2267-2268 and 2271-2272 were used for amplification of KLC and KHC cDNA, respectively. Following the cDNA amplification, KLC and KHC open reading frame (ORF)-specific nested primers containing restriction enzyme sites for directional cloning were used to amplify the ORF sequence. The nested primers used for amplification of the KLC and KHC ORFs were primers 2269 and 2270 and primers 2273 and 2274, respectively. Amplified products were cloned directly into the p2ZOp2-insect eukaryotic expression vector, which places the gene under the control of the constitutive Orgyia pseudotsugata multiple nucleopolyhedrovirus IE2 promoter (43, 44). Both clones were confirmed through restriction enzyme digestion and complete sequencing.

Cloning of KLC and KHC containing epitope tags and green fluorescent protein (GFP) fusions. T. ni KLC and KHC were cloned into the p2ZOp2 vector and were tagged with HA or Myc at both the N terminus (N-HA and N-Myc, respectively) and the C terminus (C-HA and C-Myc, respectively) by inverse PCR. Primer pairs 2350-2351, 2352-2353, 2358-2359, and 2360-2361 were used for C-HA, N-HA, C-Myc, and N-Myc tagging of KLC, respectively. Primer pairs 2338-2339, 2340-2341, 2346-2347, and 2348-2349 were used for C-HA, N-HA, C-Myc, and N-Myc tagging of KHC, respectively. Enhanced green fluorescent protein (EGFP) fusion to the C-terminal HA-tagged KLC and KHC constructs was done by using a Gibson assembly (New England BioLabs). The EGFP was PCR amplified from pFAcT-GFP (4) using primers 2380 and 2381, with each primer having a 15-nucleotide overhang homologous to the end of C-HA-KLC, which was amplified using primers 2374 and 2375. A similar strategy was used to construct the KHC C-terminal EGFP fusion. Primers 2407 and 2408 were used for PCR amplification of EGFP from pFAcT-GFP, and primers 2405 and 2406 were used for PCR amplification of C-HA-KHC. All the tagged and fusion constructs were confirmed through restriction enzyme digestion, sequencing, and Western blotting.

Construction of polyclonal stable cell lines. Stable cell lines were generated as previously described (43). Briefly, plasmid DNA (1  $\mu$ g) from the Myc- or HA-tagged KLC and KHC expression constructs with an EGFP fusion were transfected into cells of the *T. ni* Tn5B1 cell line. The transfected cells were allowed to grow for 48 h under normal medium conditions. At 48 h posttransfection (hpt), the normal medium was removed and replaced with medium containing zeocin (1 mg/ml). The cultures were maintained for 2 weeks for selection of stable transformed cells. The concentration of zeocin in the medium was reduced to 500  $\mu$ g/ml for

TABLE 1 Primers used in this study

Primer	Sequence (5' to 3')			
2267	ACAGTATTACATAATAGCCGCAT			
2268	TCAAGGTTTAACGGTTAGCAA			
2269	TCGGTACCATAATGTCGAAGACTTTGAACGCCTACAGAATAA			
2270	TTGGATCCCTACTGGTGCGGCGCATTGCTCCCAGTGTTGATC			
2271	GTAGCCCAAATGATTAAGCCTA			
2272	CCGACATTTTGATATTGCTGT			
2273	TCGAATTCTCAACTCTCATCTCGGGCGCCAACAATAAT			
2274	TTGGTACCAAAATGGCAGCTGATCGTGAGATT			
2350	CCCGACTACGCCTAGGGATCCTCTAGAGCGGCCAT			
2351	CACGTCGTAGGGGTACTGGTGCGGCGCATTGCTCCCAGTG			
2352	GCCCGACTACGCCTCGAAGACTTTGAACGCCTACA			
2353	ACGTCGTAGGGGTACATTATGGTACCAAGCTTTAAAT			
2358	TCTCCGAGGAGCACCTGTAGGGATCCTCTAGAGCGGCCAT			
2359	TCAGCTTCTGCTCCTGGTGCGCGCATTGCTCCCAGTG			
2360	TCCGAGGAGGACCTGTCGAAGACTTTGAACGCCTACA			
2361	GATCAGCTTCTGCTCCATTATGGTACCAAGCTTTAAAT			
2338	TGCCCGACTACGCCTGAGAATTCTGGATCCTCTAG			
2339	CGTCGTAGGGGTAACTCTCATCTCGGGCGCCAACAATA			
2340	GTGCCCGACTACGCCGCAGCTGATCGTGAGATTGC			
2341	GTCGTAGGGGTACATTTTGGTACCAAGCTTTAAAT			
2346	TCCGAGGAGCCTGTGAGAATTCTGGATCCTCTA			
2347	GATCAGCTTCTGCTCACTCTCATCTCGGGCGCCCAACA			
2348	TCCGAGGAGGACCTGGCAGCTGATCGTGAGATTG			
2349	GATCAGCTTCTGCTCCATTTTGGTACCAAGCTTTAAA			
2405	TGAGAATTCTGGATCCTCTAGAGCGGCCATC			
2406	GGCGTAGTCGGGCACGTCGTAGG			
2407	GTGCCCGACTACGCCGTGAGCAAGGGCGAGGAG			
2408	GATCCAGAATTCTCACTTGTACAGCTCGTCCAT			
2374	TAGGGATCCTCTAGAGCGGCCATCGATAT			
2375	GGCGTAGTCGGGCACGTCGTAGGGGTACT			
2380	GTGCCCGACTACGCCGTGAGCAAGGGCGAGGAG			
2381	TCTAGAGGATCCCTACTTGTACAGCTCGTCCAT			
2445	AAGAGATCGAATTAGCTATGGCAGCTGATCGTGAGATTG			
2446	TATAGGGCTCTAGAGACTCTCATCTCGGGCGCCAACAATA			
2447	AAGAGATCGAATTAGCTATGTCGAAGACTTTGAACGCCTA			
2448	TATAGGGCTCTAGAGCTGGTGCGGCGCATTGCTCCCAGTG			
2449	TGACTGTATCGCCGGCTATGGCAGCTGATCGTGAGATTG			
2450	TATAGGGCTCTAGAGACTCTCATCTCGGGCGCCCAACAATA			
2451	TGACTGTATCGCCGGCTATGTCGAAGACTTTGAACGCCTA			
2452	TATAGGGCTCTAGAGCTGGTGCGGCGCATTGCTCCCAGTG			
2453	AAGAGATCGAATTAGCTGGCTACGAGATCCCGGCGCGCTG			
2454	TGACTGTATCGCCGGCTGGCTACGAGATCCCGGCGCGCTG			
2457	AAGAGATCGAATTAGCTGGTGGTTCATTAGCTCAAAAGCA			
2458	TGACTGTATCGCCGGCTGGTGGTTCATTAGCTCAAAAGCA			
2461	AAGAGATCGAATTAGCTATGGCGCTAGTGCCCGTGGGTATGG			
2462	TATAGGGCTCTAGAGGACGGCTATTCCTCCACCTGCTTCG			

culture amplification. Subsequent passes were done with medium with a reduced amount of zeocin (250  $\mu g/ml$ ) (44).

**Generation of polyclonal antibodies.** Peptide-specific polyclonal antibodies against *T. ni* KLC (amino acids 179 to 194) and AC141 (amino acids 215 to 229) were generated in rabbits by Pacific Immunology Inc.

Coimmunoprecipitation of protein complexes. Tn5B1 cells or polyclonal stably transformed cells expressing HA-tagged KLC and KHC (50  $\times 10^6$ ) were infected with either ac141KO-HA-AC141 (5) or WT virus at a multiplicity of infection (MOI) of 10. Infected cells were harvested at 24 h p.i. (hpi) and resuspended in 1.25 ml of either HEPES lysis buffer (15 mM HEPES, pH 7.6, 10 mM KCl, 0.1 mM EDTA, 0.5 mM EGTA 1 mM dithiothreitol, 1% protease inhibitor cocktail [Invitrogen]) or EBC lysis buffer (50 mM Tris-HCl, pH 8.0, 120 mM NaCl, 0.5% Nonidet P-40, 0.2 mm sodium orthovanadate, 1% sodium fluoride, 1% protease inhibitor cocktail) (5, 45). The lysates were passed through a French press twice at 1,000 lb/in² and centrifuged at 6,000  $\times$  g for 20 min at 4°C. The lysates were incubated with either an EZ<sup>view</sup> Red anti-HA affinity gel conjugated to an

anti-HA monoclonal antibody (Sigma-Aldrich) or polyclonal AC141 antibody (6 μg) diluted in 200 μl 1× phosphate-buffered saline (PBS; 136.66 mM NaCl, 2.7 mM KCl, 10 mM Na<sub>2</sub>HPO<sub>4</sub>, 1.8 mM KH<sub>2</sub>PO<sub>4</sub>). The mixture was incubated overnight at 4°C on a rotor wheel. The AC141 antibody and lysate mix was further incubated with protein G Dynabeads (Invitrogen) at 4°C on a rotor wheel for 2 h. Red affinity beads or Dynabeads bound to lysate were washed three to five times with either NETN wash buffer (20 mM Tris-HCl, pH 8.0, 1 mM EDTA, 0.5% NP-40, 150 mM NaCl) or Tris-buffered saline (TBS) wash buffer (50 mM HEPES, pH 7.6, 150 mM or 500 mM NaCl, 0.1% Triton X-100). The beads were eluted with 180 µl of elution buffer (100 mM glycine-HCl, pH 2.2), and the pH was raised with 1.5 M Tris-HCl, pH 8.8, to a final pH of 8. The eluent volume was vacuum concentrated to 60 μl and mixed with 20 μl of 4× protein sample buffer (PSB; 277.8 mM Tris-HCl, pH 6.8, 44.4% [vol/vol] glycerol, 0.02% bromophenol blue, 4% β-mercaptoethanol, 1% protease inhibitor cocktail [Sigma-Aldrich]). The sample was boiled for 10 min and subjected to SDS-polyacrylamide gel electrophoresis (PAGE) using Mini-Protean TGX stain-free gels (Bio-Rad), and the proteins were examined by Western blotting.

Western blot analysis. SDS-PAGE-separated proteins were electrotransferred onto a Millipore Immobilon membrane using a Bio-Rad transfer apparatus as recommended by the manufacturer's protocol. The membranes were blocked for 1 h in blocking solution (5% skim milk in Tris-buffered saline and Tween 20 [TBST; 50 mM Tris, 150 mM NaCl, 0.5% Tween 20]), followed by 1 h of incubation with primary antibody. The following primary antibodies were used: mouse monoclonal anti-HA conjugated to horseradish peroxidase (1:5,000; Invitrogen), rabbit polyclonal anti-T. ni KLC (1:500), rabbit polyclonal anti-AC141 (1:2,500), mouse monoclonal anti-VP39 (1:3,000), rabbit polyclonal FP25 (1: 5,000), rabbit polyclonal BV/ODV-C42 (1:5,000), and mouse monoclonal anti-β-tubulin (1:1,000; ExBio). The following secondary antibodies conjugated to horseradish peroxidase were used: rabbit anti-mouse immunoglobulin (1:10,000) and goat anti-rabbit immunoglobulin (1: 15,000) (Jackson ImmunoResearch Laboratories Inc.). Bound antibodies were detected by incubation with peroxidase-conjugated secondary antibody and detected with a Western Lightning Plus-ECL enhanced chemiluminescence system (Perkin-Elmer). Membranes were imaged in a Bio-Rad ChemiDoc MP imaging system.

Immunofluorescence microscopy. Polyclonal cell lines expressing Myc-tagged KLC and KHC fused to EGFP and Tn5B1 cells were plated on sterile coverslips and allowed to settle overnight (46). Cells were infected with either ac141KO-HA-AC141 or WT virus at an MOI of 10 to 20. At different times postinfection, cells were fixed (100 mM HEPES, 5 mM MgCl<sub>2</sub>, 5 mM EGTA, pH 6.9, 4% formaldehyde) for 45 min. The cells were permeabilized with 0.01% Triton X-100 solution in  $1 \times$  PBS for 15 min. The cells were first blocked with Image iT FX signal enhancer solution (Molecular Probes) for 30 min, followed by blocking (with 2% bovine serum albumin in 1× PBS) for an additional 30 min. Cells were incubated with the following primary antibodies: mouse monoclonal anti c-Myc-9E10 (1:50; Santa Cruz Biotechnology), rabbit polyclonal anti-HA (1:200; Abcam), rabbit polyclonal AC141 (1:500), and mouse anti-β-tubulin (1: 500; Exbio) (47, 48). After incubation with the primary antibodies, the cells were washed with blocking buffer 3 times for 10 min each time. The cells were incubated with the following secondary antibodies: goat antimouse immunoglobulin conjugated to Alexa Fluor 635 (1:500; Molecular Probes), goat anti-rabbit immunoglobulin conjugated to Alexa Fluor 488 (1:500; Molecular Probes), goat anti-rabbit immunoglobulin conjugated to Alexa Fluor 647 (1:500; Molecular Probes), and goat anti-mouse immunoglobulin conjugated to Alexa Fluor 405 (1:500, Molecular Probes). Following incubation with the secondary antibodies, the cells were washed 3 times in blocking buffer, and coverslips were mounted with Prolong Gold antifade reagent (Molecular Probes) with or without DAPI (4',6'-diamidino-2-phenylindole).

All the images were acquired with a Leica-DM IRE2 confocal laser scanning microscope (CLSM) using a  $63\times$  oil immersion lens. Samples

were sequentially excited at 488 nm for Alexa Fluor 488 or EGFP, 633 nm for Alexa Fluor 647 or Alexa Fluor 635, and 405 nm for DAPI or Alexa Fluor 405. z-stacks of sequential images 3.29  $\mu$ m apart were used to construct three-dimensional confocal images. Confocal images were analyzed using Leica software (LAS-AS or LAS-X), and deconvolution of the images was performed using the Huygens Suite (v14.1.0). Surface rendering analysis was performed using Imaris software (v7.3.1). NIH ImageJ software was used for calculating and evaluating Pearson's correlation (Rr) values and overlap coefficient (R) values for Myc-tagged cell lines infected with virus carrying HA-AC141. Correlation analysis was done on 30 regions of interests (ROIs) from 5 different cells. These ROIs were selected on the basis of the regions which had dense green or AC141 signals. Pearson's overlap coefficients for the colocalization analysis of VP39-3×mCherry nucleocapsids with microtubules were determined using the Leica LAS-X software suite.

siRNA-mediated knockdown of T. ni KLC. The stealth small interfering RNAs (siRNAs) against T. ni KLC were designed using the Block-iT RNA interference (RNAi) designer (Life Technologies). The KLC-specific siRNAs were 5'-CAGGAAGAGCAUCGAUGCUAUUGAA-3' starting at nucleotide position 198 and 5'-CAAGUACAAGGAAGCAGAGACACU A-3' starting at nucleotide position 1191 relative to the start of the KLC ORF. The negative-control nonspecific siRNA sequences were also designed by use of the Block-iT RNAi designer and were 5'-CAGGAGACU ACGUAGUAUCUAGGAA-3' and 5'-CAAACAGGAGAAGACAGAAC GUCUA-3'. The KLC-specific or control siRNAs were simultaneously transfected into the polyclonal stable cell lines expressing HA-tagged KLC at either the C or the N terminus. The polyclonal stable cell lines were plated at  $1 \times 10^6$  cells per well in a six-well tissue culture plate. The cells were transfected with each siRNA at a final concentration of 5 nM using the Lipofectin reagent (49) for 4 h at 27°C in the absence of any antibiotics. Similar conditions were maintained for cells transfected with negativecontrol siRNA. At 4 hpt, the cells were washed 3 times with TC100 medium and the medium was replaced with TC100 plus zeocin (250 µg/ml). At 24 and 48 hpt, the cells were harvested and washed twice with  $1 \times PBS$ , and the cells were lysed in 1× PSB. Samples were separated on SDSpolyacrylamide gels, and the downregulation of N- or C-HA-KLC was determined by Western blotting. The bands were quantified using Image Lab (v5.1) software (Bio-Rad).

In N- and C-HA-KLC-knockdown and infection experiments, cells were transfected with either the siRNA or negative-control siRNA using the same protocol mentioned above. At different times posttransfection, the medium was removed and the cells were infected with  $ac141{\rm KO\textsc{-}HA\textsc{-}AC141}$  at an MOI of 5 and incubated for 1 h. The cells were washed 3 times with TC100 medium, and the medium was replaced with TC100 plus zeocin (250 µg/ml). At 24 hpi, culture supernatants were collected for determination of the BV titer by the 50% tissue culture infective dose (TCID $_{50}$ ) endpoint dilution assay (50) and cells were harvested for Western blot analysis.

Yeast two-hybrid analysis. Saccharomyces cerevisiae strain YRG-2 (Stratagene) was used for yeast two-hybrid analysis as previously described (5). Genes of interest were cloned by PCR amplification, followed by use of the Gibson assembly strategy as described above and ligation into the binding domain bait vector pBD-Gal4-Cam or the activation domain prey vector pAD-Gal4-2.1 (Stratagene). The T. ni KLC was cloned both into the activation domain, using primers 2447 and 2448 (Table 1), and into the binding domain, using primers 2451 and 2452. Similarly, T. ni KHC was cloned into activation and binding domain vectors using primers 2445 and 2446 and primers 2449 and 2450, respectively. The TPR domain of KLC and the stalk/tail domain of KHC, which have been known to interact with cargo, were cloned into the activation vector pAD-Gal4-2.1 using primer pairs 2453-2448 and 2457-2446, respectively, and into the binding domain vector pBD-Gal4-Cam, using primer pairs 2454-2452 and 2458-2450, respectively (Table 1). AcMNPV VP39 was cloned into the activation domain vector using primers 2461 and 2462. Clones pAD-AC141, pBD-ΔAC141 (a mutant of AC141with a 37-amino-acid

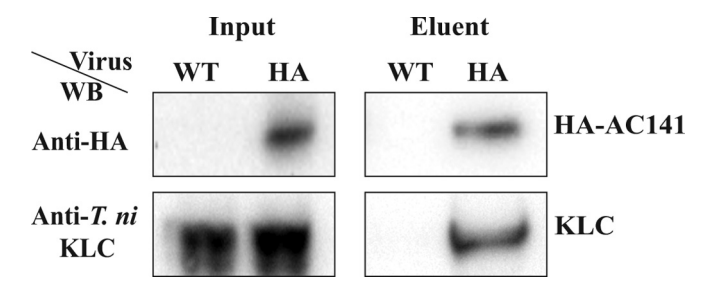


FIG 1 Coimmunoprecipitation of HA-AC141 and untagged *T. ni* KLC in infected Tn5B1 cells. Tn5B1 cells were infected with *ac141*KO-HA-AC141 (HA-AC141) or WT virus and harvested at 24 hpi, and cell lysates were coimmunoprecipitated with anti-HA beads. The input and the eluent were analyzed by Western blotting (WB) and probed with anti-HA mouse monoclonal antibody or a rabbit polyclonal anti-*T. ni* KLC antibody. In the input lanes, 0.25% of the total lysate was loaded for both blots. For the eluent blots, 4% of the total eluent was loaded for the anti-HA blot (top) and 25% of the total eluent was loaded for the anti-*T. ni* KLC blot (bottom).

deletion at the N terminus), and pBD-VP39 have been previously described (5, 6). Competent YRG-2 yeast cells were transformed with 200 ng of the desired plasmids, followed by heat shock in Tris-EDTA-lithium acetate-polyethylene glycol-dimethyl sulfoxide solution (5). Double transformants were screened for growth on minimal synthetic defined (SD) base medium plates lacking two amino acids (leucine and tryptophan) to ensure the presence of both bait and prey vectors. The screened colonies were further tested for a positive interaction by growth on minimal SD base medium plates lacking three amino acids (leucine, tryptophan, and histidine).

## **RESULTS**

Coimmunoprecipitation of HA-AC141 and T. ni KLC. It has previously been shown (17) that AC141, which is required for BV production, interacts with lepidopteran β-tubulin and the TPR domain of *D. melanogaster* kinesin-1, suggesting that baculovirus nucleocapsids may be transported using the kinesin-1 microtubule transport system (5, 18). To further investigate this association, coimmunoprecipitation experiments were performed to determine if AC141 interacts with T. ni kinesin-1 in AcMNPVinfected cells. Tn5B1 cells were infected with a virus expressing HA-tagged AC141 (ac141KO-HA-AC141) or with AcMNPV E2 wild-type (WT) virus as a control. Protein complexes were immunoprecipitated with anti-HA-labeled beads, and eluted proteins were subjected to Western blot analysis using a T. ni KLC-specific antibody (Fig. 1). The result showed that T. ni KLC specifically coimmunoprecipitated with HA-AC141 but was not detected in the eluent of cells infected with WT virus. This result provides the first evidence that the AcMNPV protein AC141 associates with the T. ni host kinesin-1. A reciprocal pulldown assay was not possible because of the low sensitivity of the polyclonal KLC antibody.

Cloning of *T. ni* kinesin-1 and generation of stable Tn5B1 cells expressing tagged KHC and KLC. To enable a more detailed analysis of the interaction between kinesin-1 and AcMNPV nucleocapsid proteins, transformed cell lines expressing tagged forms of KLC or KHC were developed. The sequences of *T. ni* KHC and KLC were originally identified by high-throughput transcriptome sequencing (RNA-seq) analysis of *T. ni* cells (42). The cDNAs were cloned, and constructs expressing KHC and KLC tagged with either the HA or the Myc epitope tag at both the N and C termini were made (Fig. 2A). Proteins were tagged at both the N and C termini to control for any possible steric hindrance caused

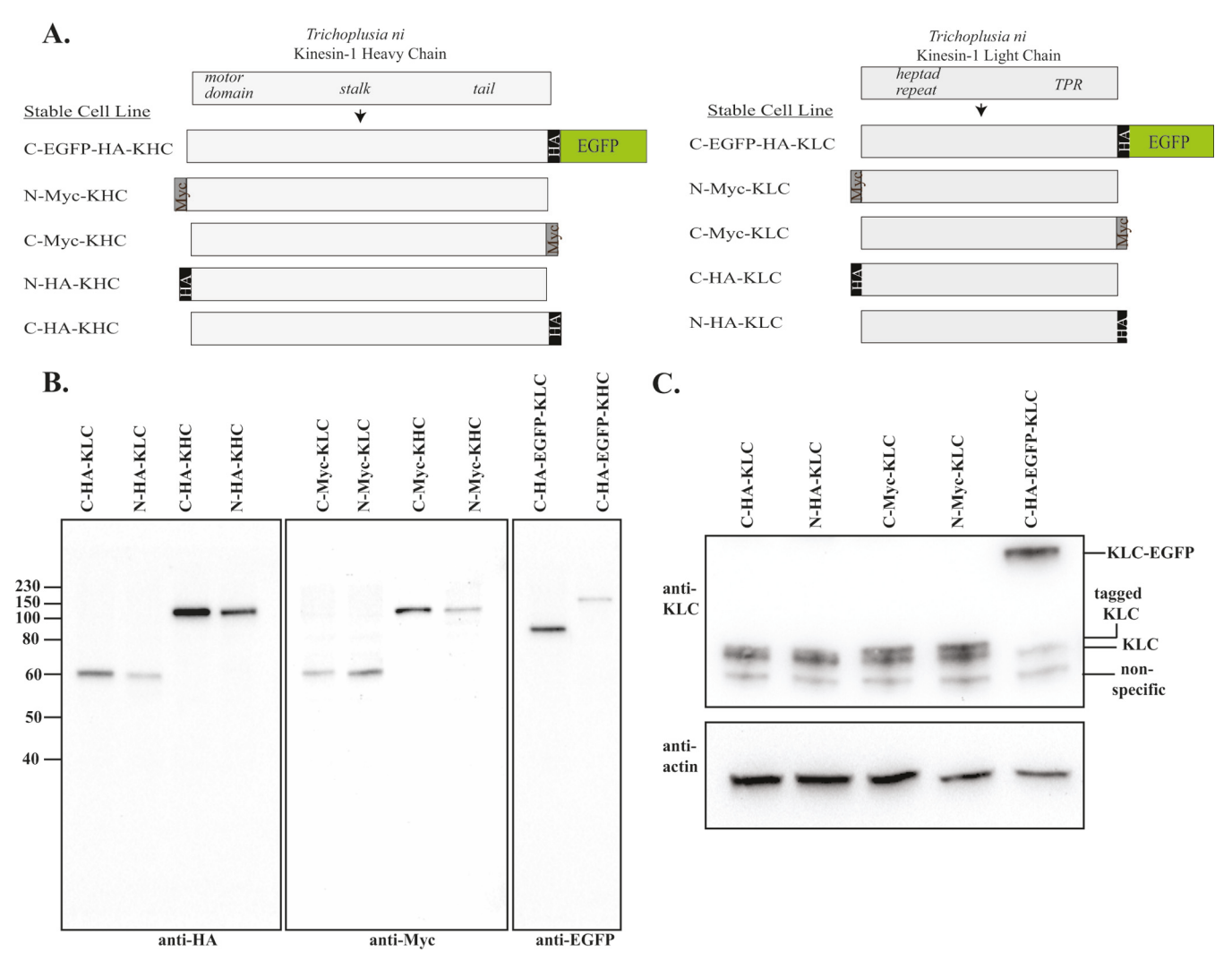


FIG 2 Constructs used to generate stable cell lines expressing *T. ni* KHC and KLC that contain epitope tags or EGFP fusions. (A) Schematic diagrams of the expressed KHC or KLC proteins in the stable cell lines indicated on the left. The expressed proteins were tagged at either the N or C terminus with a Myc tag (gray) or an HA tag (black). In addition, two cell lines were generated that had EGFP fused to the C-HA-KHC and C-HA-KLC constructs at the C terminus (green). The relative locations of the motor, stalk, and tail domains in KHC and the heptad repeat and TPR domains in KLC are also indicated. (B) Total protein from polyclonal stably transformed cells was subjected to SDS-PAGE, and the expression of tagged KLC and KHC was analyzed by Western blotting. The HA and Myc tags and the EGFP fusion were detected with the corresponding antibodies, indicated below each blot. Numbers to the left of the gel are molecular masses (in kilodaltons). (C) (Top) Total protein from polyclonal stable cell lines expressing tagged KLC were subjected to SDS-PAGE, and the expression of endogenous KLC and engineered KLC was analyzed by Western blotting with a polyclonal antibody against *T. ni* KLC. (Bottom) The loading control, which is the same blot shown at the top of panel C probed with anti-actin antibody.

by the epitope tag. Additional KHC and KLC constructs that were tagged at the C terminus with both the HA epitope tag and EGFP were made. Each of these constructs was used to generate stably transformed Tn5B1 polyclonal cell lines.

The transformed cell lines were named by use of the expressed protein and the location of the attached tag or fusion protein (Fig. 2A). The stable expression of tagged KHC or KLC was confirmed by Western blotting (Fig. 2B). The levels of expression of both endogenous KLC and tagged KLC in the cell lines stably expressing KLC were compared (Fig. 2C).

**Coimmunoprecipitation of HA-tagged KLC or KHC and AC141.** To further confirm the association of AC141 and *T. ni* kinesin-1, stable cell lines expressing tagged forms of KLC or KHC were used. Stable cell lines expressing C-HA-KLC or N-HA-KLC

(the C-HA-KLC and N-HA-KLC cell lines, respectively) (Fig. 2) were initially infected with WT virus. Protein complexes were pulled down either with polyclonal AC141 antibody or with preimmune serum as a control. The results showed that on immuno-precipitation with anti-AC141, both C-HA-KLC and N-HA-KLC were coimmunoprecipitated. Neither C-HA-KLC nor N-HA-KLC was coimmunoprecipitated with the control preimmune serum (Fig. 3A). The same eluents from cell lines expressing C-HA-KLC or N-HA-KLC but not those from control samples also specifically eluted  $\beta$ -tubulin when AC141 was pulled down (Fig. 3A), further providing evidence for an association between AC141, KLC, and  $\beta$ -tubulin. The coimmunoprecipitation of AC141 and  $\beta$ -tubulin was previously shown using recombinant virus expressing HA-tagged AC141 (17). The current experiments

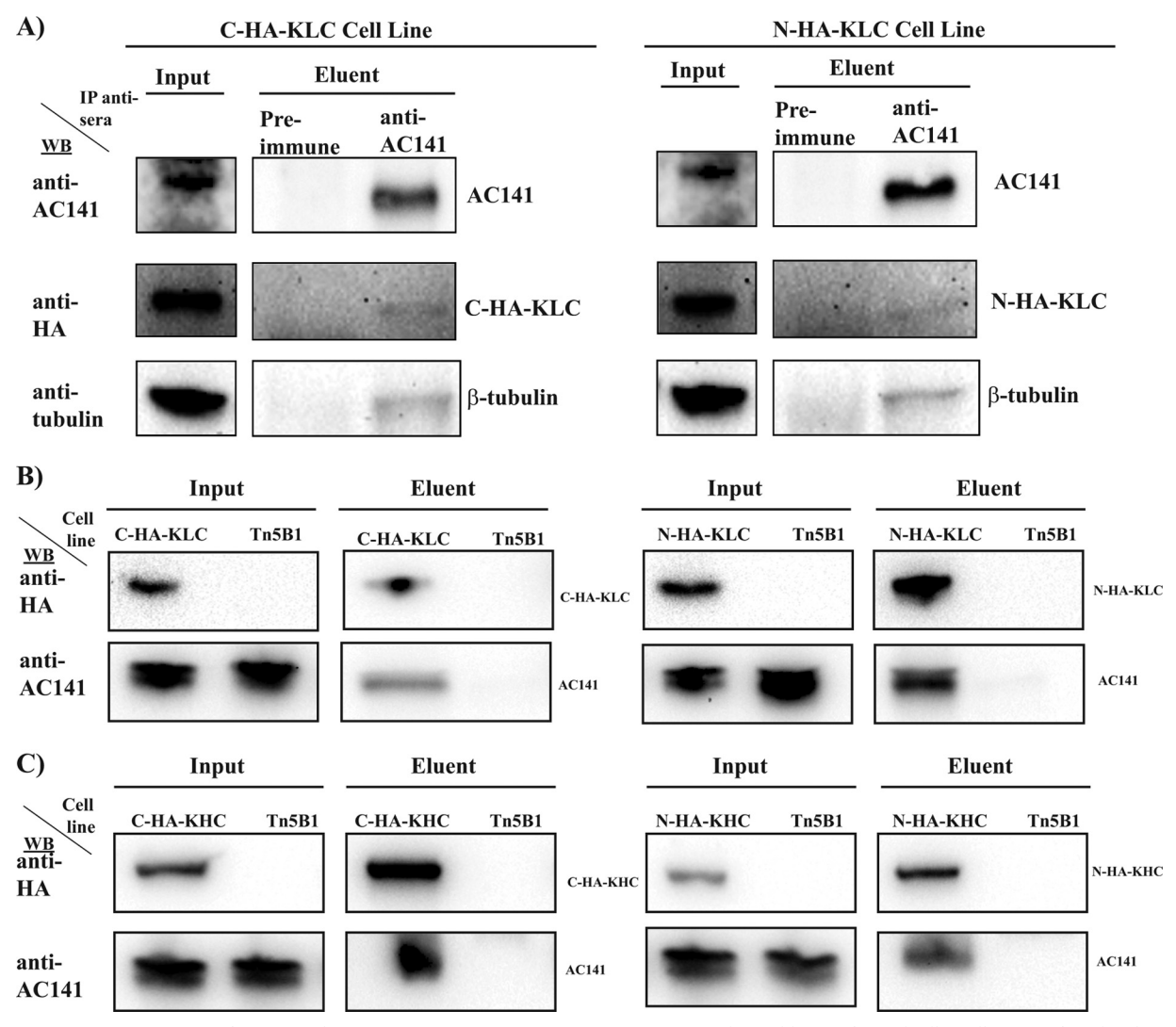


FIG 3 Coimmunoprecipitation of AC141 with C- or N-HA-KLC or C- or N-HA-KHC expressed in stably transformed cells. Cells were infected with WT virus and harvested at 24 hpi; coimmunoprecipitated protein complexes were subjected to Western blotting (WB) and probed with the antibodies shown on the left. Input lanes were loaded with 0.25% of the total input for every blot. (A) Cells of the C- or N-HA-KLC cell line were infected with WT virus, and protein complexes were coimmunoprecipitated with anti-AC141 rabbit polyclonal antibody or the control preimmune serum. Eluent lanes contained 4% of the total eluent for the HA-tagged KLC and  $\beta$ -tubulin blots. IP, immunoprecipitation. (B) Cells of the C-HA-KLC- or N-HA-KLC cell line or control Tn5B1 cells were infected with WT virus, and protein complexes were coimmunoprecipitated with anti-HA beads. Eluent lanes contained 4% of the total eluent for the C- and N-HA-KLC blots and 25% of the total eluent for the AC141 blot. (C) Cells of the C-HA-KHC- or N-HA-KHC cell line or Tn5B1 cells were infected with WT virus, and protein complexes were coimmunoprecipitated with anti-HA beads. The eluent lanes contained 4% of the total eluent for the C- and N-HA-KHC blots and 25% of the total eluent for the AC141 blot. (C) was used as a loading control (not shown).

confirmed these results using WT virus-infected cells and anti-AC141 polyclonal antisera.

Reciprocal coimmunoprecipitations were performed using the C-HA-KLC and N-HA-KLC cell lines infected with WT virus and immunoprecipitated using anti-HA beads (Fig. 3B). As a control, Tn5B1 cells were infected with WT virus. The immunoprecipitated complexes were analyzed by Western blotting and probed with anti-AC141. The results showed equal levels of AC141 in input lanes of Tn5B1 and C-HA-KLC or Tn5B1 and N-HA-KLC WT virus-infected cell lines; however, coimmunoprecipitation of AC141 was observed only in cells of the C-HA-KLC and N-HA-KLC cell lines (Fig. 3B). The reciprocal coimmunoprecipitation of HA-KLC and AC141 further confirmed the association of KLC and AC141.

Kinesin-1 is a tetramer of two KLC and two KHC molecules. Therefore, if AC141 is associated with kinesin-1, both KHC and KLC should be coimmunoprecipitated with AC141. Therefore, to confirm the association of kinesin-1 with AC141, coimmunoprecipitation experiments were performed with cells expressing KHC tagged with HA at the C and N termini, as was done with KLC. Cell lines stably expressing C-HA-KHC and N-HA-KHC (the C-HA-KHC and N-HA-KHC cell lines, respectively) and Tn5B1 cells, which were used as a control, were infected with WT virus, and protein complexes were immunoprecipitated with anti-HA beads and analyzed by Western blotting. As was shown for KLC, the results showed that HA-KHC was immunoprecipitated only in the C-HA-KHC and N-HA-KHC cell lines (Fig. 3C). AC141 was detected in the input of WT virus-infected C-HA-KHC, N-HA-

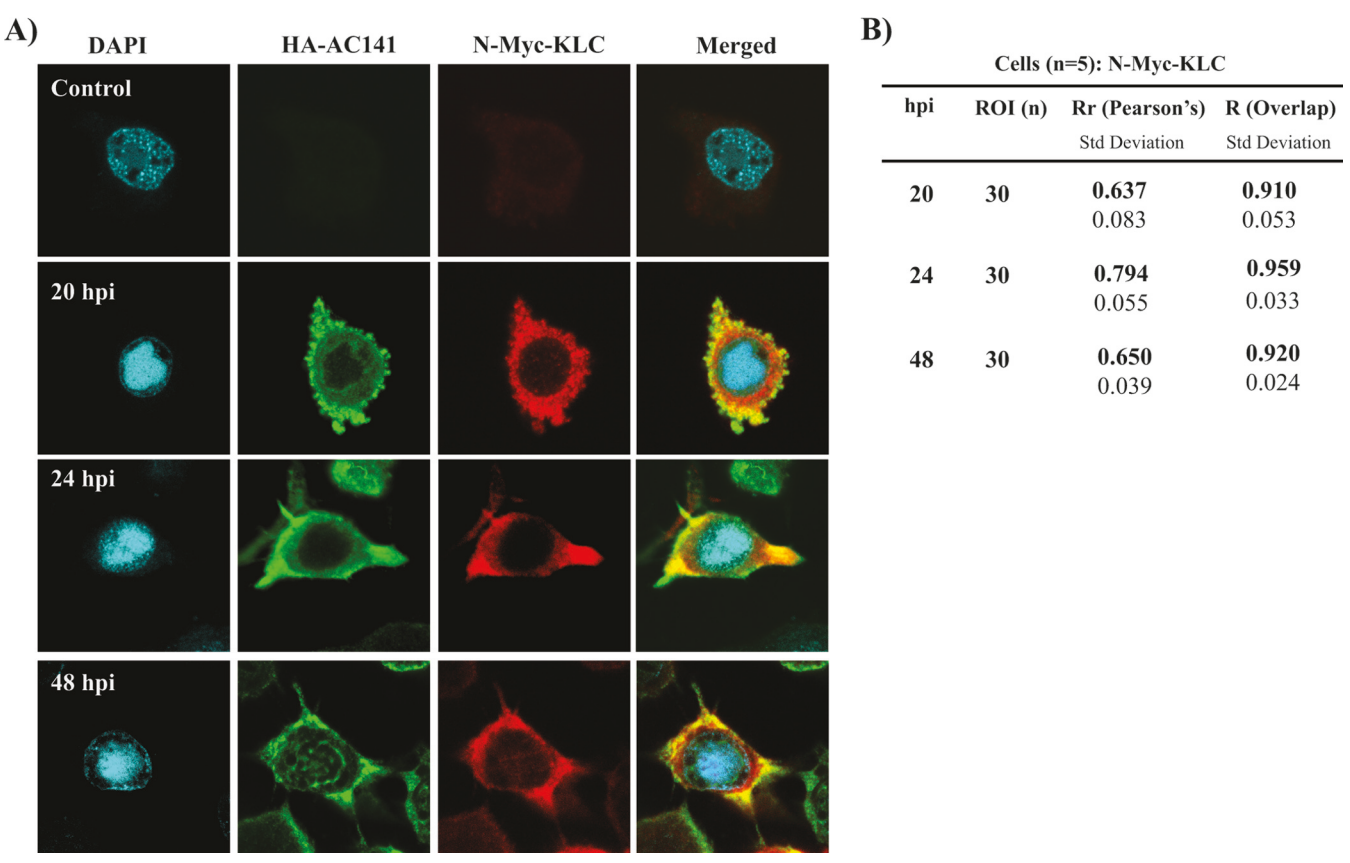


FIG 4 Colocalization analysis of HA-AC141 and *T. ni* Myc-KLC at 20, 24, and 48 hpi. (A) Cells of the N-Myc-KLC cell line were infected with *ac141*KO-HA-AC141 and fixed at 20, 24, and 48 hpi. Nuclei were stained with DAPI (blue), and HA-AC141 was detected with rabbit polyclonal anti-HA and goat anti-rabbit immunoglobulin antibodies conjugated to Alexa Fluor 488 (green). N-Myc-KLC was detected with mouse monoclonal anti-Myc and goat anti-mouse immunoglobulin antibodies conjugated to Alexa Fluor 635 (red). (B) The *Rr* and *R* values for 30 ROIs from 5 different cells were calculated at each time point for N-Myc-KLC and HA-AC141.

KHC, and Tn5B1 cells. However, AC141 was specifically coimmunoprecipitated only for the C-HA-KHC and N-HA-KHC cell lines (Fig. 3C). The coimmunoprecipitation of AC141 with *T. ni* KLC and KHC confirms that kinesin-1 potentially interacts either with free AC141 or with a protein complex that contains AC141. Since AC141 is a nucleocapsid-associated protein, the protein complex could include viral nucleocapsids.

Analysis of T. ni KLC or KHC colocalization with AC141. The coimmunoprecipitation experiments showed that AC141, which is a nucleocapsid protein required for viral egress, associates with kinesin-1. To further investigate this association and to identify where in the cell the interactions occur, experiments determining colocalization in infected cells were performed using confocal microscopy. For these experiments, cells expressing N-Myc-KLC (N-Myc-KLC cells) were infected with ac141KO-HA-AC141 and analyzed at 20 hpi, 24 hpi, and 48 hpi (Fig. 4). As described above, HA-AC141 (Fig. 4A, green signal) was concentrated at the cellular periphery and outside the virogenic stroma closer to the nuclear envelope. N-Myc-KLC (Fig. 4A, red signal) was ubiquitously expressed in the cytoplasm but was expressed at very low levels in the nucleus. Analysis of HA-AC141 and N-Myc-KLC colocalization at different time points showed that they colocalized in the cytoplasm and predominantly near the plasma membrane (Fig. 4A, Merged, yellow signal). HA-AC141 did not

significantly colocalize with N-Myc-KLC inside the nucleus (Fig. 4A). As a control, Tn5B1 cells were infected with WT virus, and staining and imaging conditions were the same as those described above (Fig. 4A). Negligible background fluorescence was observed for both HA-AC141 and N-Myc-KLC. Pearson's coefficient (*Rr*) and overlap coefficient (*R*) values were also calculated at 30 different ROIs to measure the efficiency colocalization and to quantify the colocalization. The *Rr* values for the colocalization of HA-AC141 and N-Myc-KLC were between 0.64 and 0.79 and the *R* values were between 0.91 and 0.96, suggesting a strong colocalization between the two proteins (Fig. 4B). These experiments were repeated with cell line C-Myc-KLC, and colocalization patterns and colocalization coefficient values for HA-AC141 and C-Myc-KLC were similar to those obtained with HA-AC141 and N-Myc-KLC (data not shown).

To confirm the association of AC141 with kinesin-1, it was necessary to determine if AC141 also colocalizes with KHC. Therefore, the N-Myc-KHC cell lines were infected with *ac141*KO-HA-AC141, fixed, and stained at 20 hpi, 24 hpi, and 48 hpi (Fig. 5A). As expected, HA-AC141 (Fig. 5A, green signal) showed nuclear and cytoplasmic localization, being concentrated around the virogenic stroma and the cellular periphery, respectively, at different time points. The localization pattern of N-Myc-KHC (Fig. 5A, red signal) was similar to that of N-Myc-KLC, and it was observed

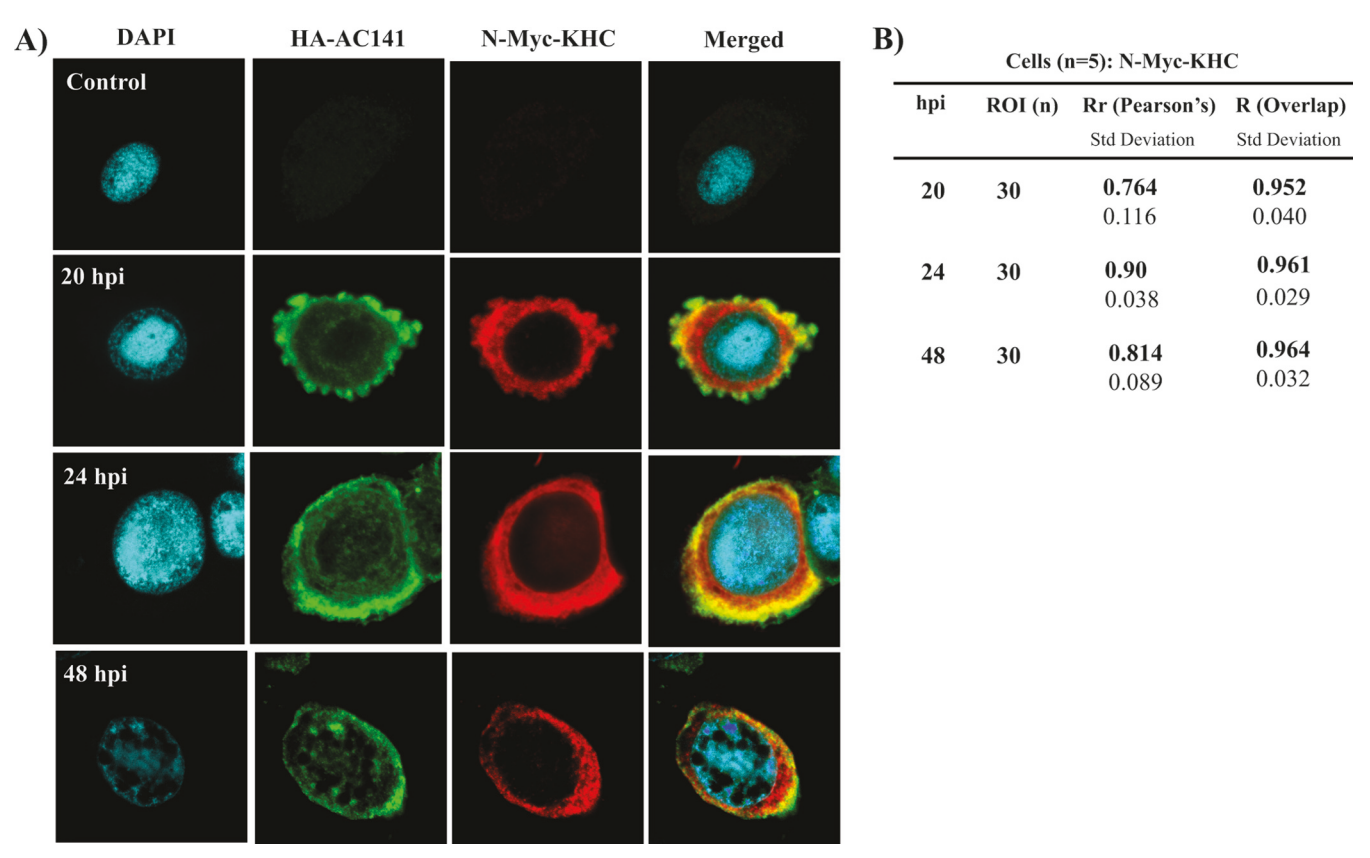


FIG 5 Colocalization analysis of HA-AC141 and *T. ni* Myc-KHC at 20, 24, and 48 hpi. (A) Cells of the N-Myc-KHC cell line were infected with *ac141*KO-HA-AC141 and fixed at 20, 24, and 48 hpi. Nuclei were stained with DAPI (blue), and HA-AC141 was detected with rabbit polyclonal anti-HA and goat anti-rabbit immunoglobulin antibodies conjugated to Alexa Fluor 488 (green). N-Myc-KHC was detected with mouse monoclonal anti-Myc and goat anti-mouse immunoglobulin antibodies conjugated to Alexa Fluor 635 (red). (B) The *Rr* and *R* values for 30 ROIs from 5 different cells were calculated at each time point for N-Myc-KHC and HA-AC141.

throughout the cytoplasm. The merged fields in Fig. 5A show regions of colocalized HA-AC141 and N-Myc-KHC (yellow) toward the cellular periphery at each time point. The nuclear HA-AC141 did not colocalize with N-Myc-KHC at 20, 24, and 48 hpi. Control Tn5B1 cells infected with WT virus had negligible background fluorescence for HA-AC141 and N-Myc-KHC (Fig. 5A). The *Rr* values ranged from 0.76 to 0.90, and the *R* values ranged from 0.95 to 0.96. These values indicate a very strong colocalization or association between HA-AC141 and N-Myc-KHC (Fig. 5B). These experiments were repeated with the C-Myc-KHC cell line, and colocalization patterns and colocalization coefficient values for HA-AC141 and C-Myc-KHC were similar to those obtained with HA-AC141 and N-Myc-KHC (data not shown).

Studies of KLC or KHC colocalization with AC141 and microtubules. The results presented above show that the kinesin-1 proteins KLC and KHC associate with AC141 at the cellular periphery. As kinesin-1 is used to transport cargo along microtubules, we wanted to determine if KHC or KLC and AC141 colocalize with microtubules. For these experiments, cells stably expressing KLC-EGFP and KHC-EGFP (stable KLC-EGFP and KHC-EGFP cells, respectively) were infected with WT virus, fixed at 24 hpi, and analyzed for the colocalization of KLC or KHC with AC141 and  $\beta$ -tubulin (microtubules). As was observed with the Myc-tagged proteins (Fig. 4 and 5), both KLC-EGFP and KHC-EGFP localized throughout the cytoplasm (Fig. 6A and B). Micro-

tubules were detected using a β-tubulin antibody and were found to be localized throughout the cytoplasm, with a concentration toward the cellular periphery being seen, similar to what has been previously observed (17, 51). Colocalization of the green fluorescence of KHC-EGFP or KLC-EGFP with the cyan staining of β-tubulin results in blue pixels in the merged image, which were observed mainly at the cellular periphery, where the microtubules were the most concentrated. The AC141 staining is shown in red (Fig. 6A and B), and it was found that AC141 colocalized with KHC-EGFP or KLC-EGFP primarily at the cellular periphery (yellow), as was observed in cells expressing Myc-tagged KLC or KHC and HA-AC141 (Fig. 4 and 5). The colocalization of AC141 (red) with β-tubulin (cyan) and KHC-EGFP or KLC-EGFP (green) results in pink pixels. Distinct pink pixels in both the single confocal plane and the z-stack were observed at the cellular periphery at the plasma membrane (Fig. 6A and B). These z-stack images, including the enlarged images, give a clear view of the microtubule structures and the colocalization of microtubules with KLC-EGFP or KHC-EGFP. The greatest degree of colocalization of all three proteins was observed at the cellular periphery adjacent to the plasma membrane. Numerous bulges, which are potential viral budding sites, were seen on the cell surface. Similar bulged regions were observed through time-lapse microscopy in infected Sf21 cells at 18 to 22 hpi (52). The bulges predominantly had either KLC or KHC and AC141 but only limited β-tubulin. The majority of co-

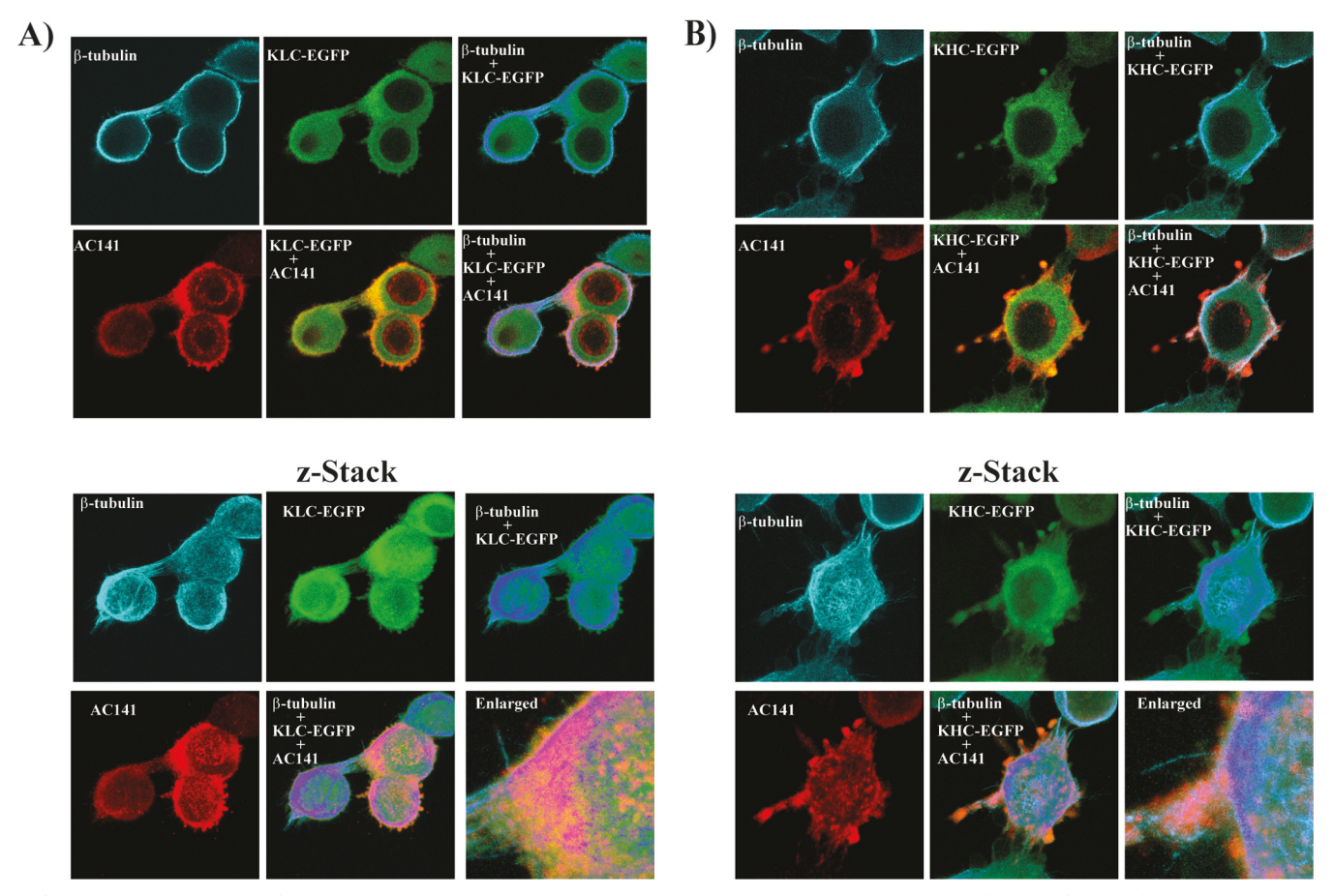


FIG 6 Colocalization analysis of AC141, KLC- or KHC-EGFP, and microtubules. KLC-EGFP (A) or KHC-EGFP (B) cells were infected with WT virus at an MOI of 10, and cells were fixed at 24 hpi. AC141 was detected with rabbit polyclonal anti-AC141 and goat anti-rabbit immunoglobulin conjugated to Alexa Fluor 647 (red).  $\beta$ -Tubulin was detected with anti- $\beta$ -tubulin mouse monoclonal antibody and goat anti-mouse immunoglobulin antibody conjugated to Alexa Fluor 405 (cyan). KLC- or KHC-EGFP is shown in green. The colocalization of  $\beta$ -tubulin with KLC- or KHC-EGFP gives blue pixels, and the colocalization of all three proteins results in pink pixels. (Top) Single two-dimensional images; (bottom) three-dimensional representations of a merged z-stack of the same cells in the top panels.

localization of all three proteins occurred below the bulges. These results suggest that AC141, kinesin-1, and microtubules colocalize at the peripheral regions of the cytoplasm near the plasma membrane and potential viral budding sites.

siRNA downregulation of KLC and impact on BV production. The coimmunoprecipitation and colocalization studies indicate that microtubules and kinesin-1 are potentially involved in the transport of nucleocapsids to the viral budding sites at the cell plasma membrane. If this is correct, the downregulation of kinesin-1 should decrease BV production. We therefore used siRNA to downregulate the cellular KLC of kinesin-1.

To confirm the downregulation of KLC by siRNA, stable polyclonal N-HA-KLC cell lines were transfected with two siRNAs and KLC expression levels were analyzed by Western blotting. The results showed that the target siRNA significantly downregulated N-HA-KLC at 24 and 48 hpt compared to N-HA-KLC expression in untreated cells or cells transfected with nonspecific siRNA (Fig. 7A). The level of N-HA-KLC expression in siRNA-treated cells was only 4% and 1% of that in untreated cells (in which it was considered to be 100%) at 24 hpt and 48 hpt, respectively. Nonspecific siRNA was observed to decrease the level of N-HA-KLC expression at 24 hpt, but the levels had nearly fully recovered by 48

hpt. The downregulation of N-HA-KLC by siRNA had no impact on cell viability or the cell growth rate (data not shown). These results showed that KLC could be downregulated by siRNA in Tn5B1 cells and could be used to assay the impacts of KLC on BV production.

To assess the impact of the downregulation of KLC on BV production, cells of the N-HA-KLC stable cell line were transfected with specific or nonspecific siRNA followed by infection with ac141KO-HA-AC141. Cells and medium were harvested at 24 hpi and 28, 36, 48, or 72 hpt. Cells were analyzed for N-HA-KLC and HA-AC141 expression (Fig. 7B), and the medium was analyzed for BV production (Fig. 7C). The downregulation of N-HA-KLC in siRNA-treated cells was observed by Western blotting at 36, 48, and 72 hpt. The downregulation of N-HA-KLC had no effect on the expression level of the late gene HA-AC141, which shows that there was no effect on the early stages of virus infection, such as the initiation of viral DNA replication. However, the BV titer in siRNA-treated cells compared to that in untreated cells showed statistically significant reductions of 81.1%, 77.5%, and 63.9% at 36, 48, and 72 hpt, respectively (Fig. 7C). For the samples tested at 28 hpt, siRNA-treated cells showed a decrease in the level of BV production of 48.5% compared to that for untreated cells,

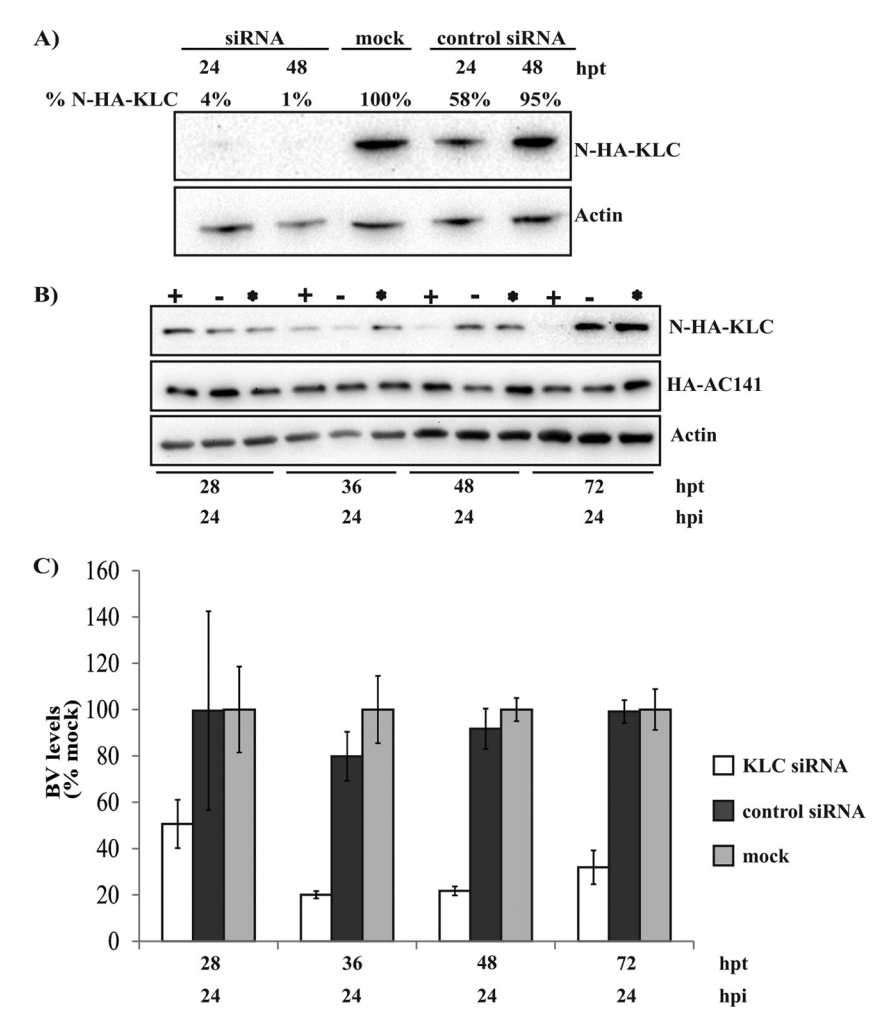


FIG 7 siRNA downregulation of *T. ni* HA-KLC expression and the impact on AcMNPV BV production. (A) Cells of the N-HA-KLC cell line were transfected with two KLC siRNAs (siRNA) or two nonspecific control siRNAs (control siRNA) or were mock transfected (mock). At 24 and 48 hpt, cells were harvested and total cell lysates were subjected to Western blotting and probed with anti-HA to detect the expression of N-HA-KLC. Actin was detected with an anti-actin antibody as a loading control. The percentage above each lane shows the levels of N-HA-KLC relative to that in untreated mock-transfected cells, which were given a value of 100%. The levels were determined using Image Lab (v5.1) software. (B) Cells of the N-HA-KLC cell line were transfected with KLC-specific siRNA (lanes +) or nonspecific control siRNA (lanes –) or were untreated and mock transfected (lanes \*). At 4, 12, 24, and 48 h after siRNA transfection, the cells were infected with *ac141*KO-HA-AC141. Supernatants and cells were harvested at 24 hpi. Total cell lysates of infected cells were subjected to Western blotting and probed with anti-HA to analyze the expression levels of N-HA-KLC and HA-AC141. Membranes were reprobed for actin as a loading control. (C) BV levels in supernatants were determined by TCID<sub>50</sub> endpoint dilution assay and are presented as a percentage of the value for the untreated control, which was given a value of 100%. BV titers are the averages from two biological replicates, each of which was performed with two technical replicates.

but the decrease was nonsignificant compared to that for nonspecific siRNA-treated cells. The BV titer did not change significantly for cells treated with negative-control siRNA at any time point. The same experiment was performed on the C-HA-KLC stable cell line, and trends similar to those described above were obtained, with BV titers being reduced after treatment with KLC siRNA (data not shown).

Association of nucleocapsid proteins VP39, BV/ODV-C42, and FP25 with KLC. The data presented above suggest that AC141 and kinesin-1 associate with each other. Therefore, if kinesin-1 associates with nucleocapsid-associated AC141, then coimmuno-precipitation of kinesin-1 should also pull down other nucleocapsid proteins. We therefore performed additional coimmunoprecipitation experiments using the C-HA-KLC and N-HA-KLC cell lines and Tn5B1 cells infected with WT virus. The coimmunoprecipitated protein complexes recovered were analyzed by Western

blotting for the nucleocapsid-associated proteins VP39, BV/ODV-C42, and FP25 (Fig. 8). The results showed N- and C-HA-KLC in the input and also in the eluent from stable C-HA-KLC and N-HA-KLC cells but not Tn5B1 cells, as expected. The other nucleocapsid proteins, VP39, BV/ODV-C42, and FP25, were also detected in all cell lines. Analysis of the eluent showed that all three nucleocapsid proteins were specifically coimmunoprecipitated from the infected C-HA-KLC- and N-HA-KLC-expressing cells (Fig. 8). VP39, BV/ODV-C42, and FP25 were not coimmunoprecipitated from Tn5B1 cells, which did not contain HA-tagged KLC. These results suggest that the coimmunoprecipitation of kinesin-1 immunoprecipitates nucleocapsids.

Association of VP39-3×mCherry nucleocapsids with microtubules. Previous studies have shown that the coexpression of WT VP39 with a VP39 fused with three copies of the mCherry fluorescent protein (VP39-3×mCherry) can be used to tag and identify

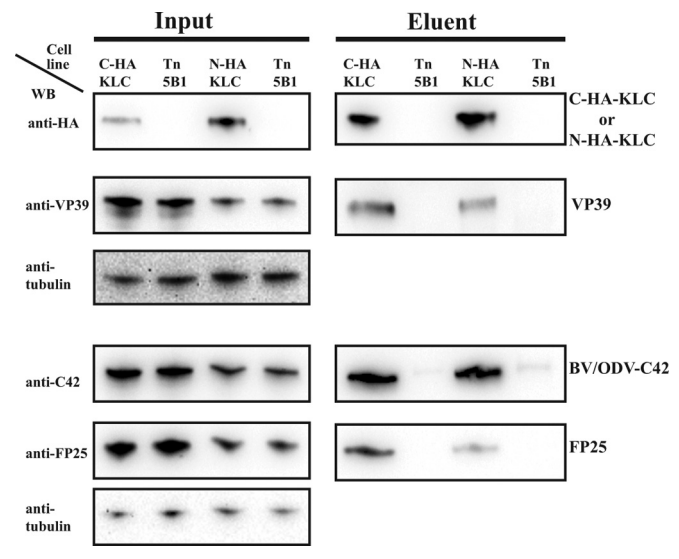


FIG 8 Association of nucleocapsid proteins VP39, FP25, and BV/ODV-C42 with C-HA-KLC or N-HA-KLC. Analysis of coimmunoprecipitation of VP39, FP25, and BV/ODV-C42 with N- or C-HA-KLC. Tn5B1 and C- or N-HA-KLC cells were infected with WT virus at an MOI of 10, the cells were harvested at 24 hpi, and protein complexes were coimmunoprecipitated with anti-HA beads and analyzed by Western blotting by probing with the antibodies indicated on the left. The VP39 and BV/ODV-C42 blots were reprobed with anti-β-tubulin as a loading control. The input lanes contained 0.25% of the total lysate, and the eluent lanes contained 25% of the total eluent.

individual nucleocapsids being actively transported on actin filaments during virus entry (11). Therefore, we compared the localization of nucleocapsids tagged with VP39-3×mCherry with that of microtubules. We examined colocalization during entry (0.5 hpi) and during egress (24 hpi) (Fig. 9A). At 0.5 hpi, nucleocapsids (Fig. 9A, red foci) were easily observed in the cytoplasm, as has been previously reported (11), but the majority (Fig. 9A, white pixels, top right) did not colocalize with microtubules. In contrast, during egress (24 hpi) the majority of VP39-3×mCherry-tagged nucleocapsids colocalized with microtubules (Fig. 9A, white pixels, top right). To quantify colocalization with microtubules during entry and egress, the total number of nucleocapsids in the cytoplasm during entry (0.25 and 0.5 hpi) and egress (20 and 24 hpi) was calculated (Fig. 9B). During entry, only 10.7% of the tagged nucleocapsids colocalized with microtubules. However, in dramatic contrast, approximately 79.3% of the nucleocapsids colocalized with microtubules during egress.

By 30 hpi, the vast majority of the VP39-3×mCherry was observed inside the nucleus, where it formed filamentous bands, which can clearly be seen in the maximum-intensity z-stack projections (Fig. 9C). Potentially similar nuclear filamentous structures have previously been observed in cells infected with a virus expressing VP39 fused to EGFP (53). The thicker part of these structures is found surrounding the virogenic stroma, with the thinner filaments permeating the stroma in the regions of low nucleic acid density, as detected by staining with DAPI. This is more clearly seen in a three-dimensional surface rendering of the nucleus (Fig. 10). The thin filaments of VP39-3×mCherry correlate with the nucleocapsid assembly sites within the virogenic stroma. The thick bands on the outside would therefore appear to be the regions of nucleocapsid concentration and ODV assembly

once they are transported from the virogenic stroma (see electron micrographs of the WT virus-infected nucleus in Fig. 10D and E). Far fewer cytoplasmic nucleocapsids were observed at 30 hpi, but most remained associated with microtubules (Fig. 9C, arrows).

Yeast two-hybrid analysis of the nucleocapsid proteins AC141 or VP39 with KLC or KHC. It has been reported previously by Danguah et al. (18) that AC141 and VP39 interact directly with the TPR motif of KLC of D. melanogaster, as determined by FRET-FILM analysis. Therefore, to further examine the association of nucleocapsid proteins with T. ni kinesin-1 molecules, we used a yeast two-hybrid system to determine whether a direct interaction between AC141 or VP39 and KLC or KHC could be detected. A similar approach has been used to show that the vaccinia virus A36R membrane protein interacts directly with the TPR domain of KLC and that the US11 protein of HSV interacts directly with stalk/tail domain of KHC (27, 33). The combinations of the bait and prey constructs used and the results of the interactions are shown in Table 2. The AC141 and KLC fusion with the binding domain showed autotransactivation. A previous analysis showed that deletion of the first 37 amino acids eliminates autoactivation, and a construct with this deletion was used in the yeast two-hybrid bait vector (ΔAC141) (6). In addition to fulllength T. ni KLC or T. ni KHC, the TPR domain of KLC and the stalk/tail domain of KHC were cloned into both the activation and binding domains. The overall results showed no direct interaction of KLC, KHC, or their TPR or stalk/tail domains with either AC141 or VP39. Yeast two-hybrid analysis using FP25 and BV/ ODV-C42 fused to the binding domain also did not show any interaction with KHC or KLC (data not shown). Analysis with positive-control T. ni KHC and KLC showed a direct interaction between these two molecules, which confirms that these clones combine to form kinesin-1. Colocalization and coimmunoprecipitation experiments showed that kinesin-1 proteins associate either with free AC141 or with nucleocapsid-associated AC141. However, the yeast two-hybrid experiments did not demonstrate direct interactions between AC141 and KHC or KLC. This suggests that either other nucleocapsid proteins are involved in the kinesin-1 interaction or host cargo adaptor proteins are required.

## **DISCUSSION**

AcMNPV and other alphabaculoviruses are known to use actin polymerization and depolymerization during entry to transport nucleocapsids to the nucleus upon infection by either BV or ODV (11, 54). However, the egress mechanism by which nucleocapsids escape the nucleus and migrate to the plasma membrane and bud to form BV remains to be resolved. Previous studies have shown that the AcMNPV protein AC141, a nucleocapsid-associated protein, is specifically required for BV production. In addition, it was found that AC141 coimmunoprecipitated β-tubulin and colocalized with microtubules. Recently, it was also shown that AC141 appeared to interact directly with the D. melanogaster KLC TPR domain (17, 18). These prior studies therefore suggested that Ac-MNPV utilizes kinesin-1 motor proteins and microtubules for nucleocapsid transport during egress, in contrast to actin polymerization, which is used during entry. In the current study, we further investigated this model by examining whether AC141 and other nucleocapsid proteins interact with kinesin-1 from the natural host T. ni, and we asked directly whether kinesin-1 is necessary for BV production. Our results show the close association of

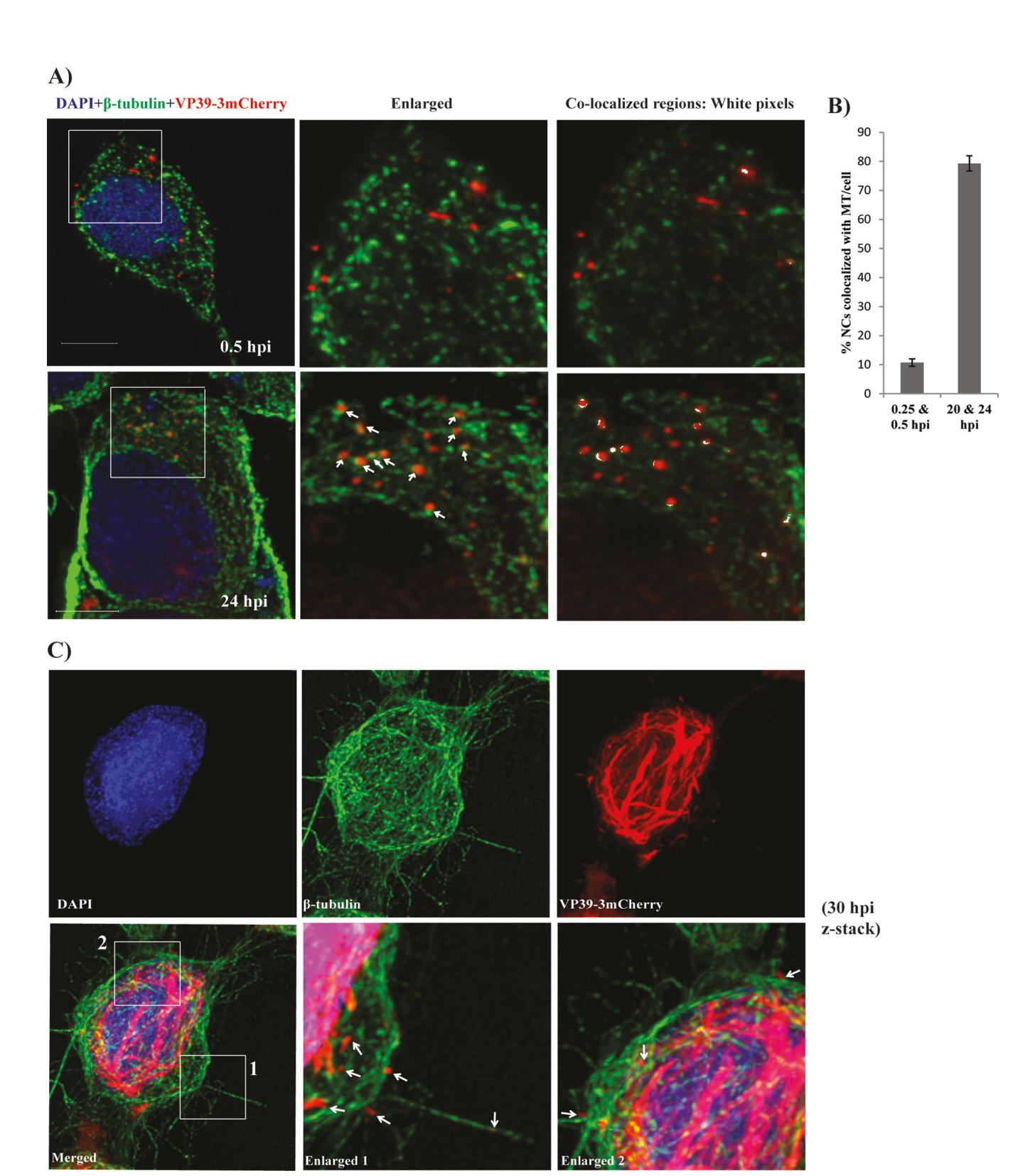


FIG 9 Colocalization of VP39-3×mCherry nucleocapsids with microtubules during entry and egress. (A) Tn5B1 cells infected with VP39-3×mCherry showing mCherry-labeled nucleocapsids (red) during entry at 0.5 hpi (top) and during egress at 24 hpi (bottom). Bars = 5 μm. Each panel is a z-stack maximum projection of 6 to 7 sections that encompasses the entire fluorescence of each NC. The microtubules were detected with mouse monoclonal antibody against β-tubulin and the corresponding secondary antibody, goat anti-mouse immunoglobulin antibody conjugated to Alexa Fluor 488 (green). The nucleus is stained with DAPI (blue). The enlarged region (center) shows potential regions of colocalization by the presence of yellow pixels (white arrows). White pixels (right) show regions of maximum colocalization, as determined by Pearson's coefficients of overlap (Leica confocal LAS X software). DAPI staining is not shown in the enlarged images. (B) Comparison of the average percentage of cytoplasmic VP39-3×mCherry nucleocapsids (NCs) that colocalize with microtubules (MTs) at 0.25 and 0.5 hpi and 20 and 24 hpi. Each bar of the graph represents the results for nucleocapsids from a total of 10 cells. Error bars represent standard errors of the means. (C) Confocal microscopy of Tn5B1 cells infected with VP39-3×mCherry at an MOI of 10 and fixed at 30 hpi. The image is a z-stack maximum projection through the entire cell showing the extensive ribbon structure of VP39-3mXCherry through the nuclear virogenic stroma. Arrows in enlarged panels 1 and 2, locations of cytoplasmic nucleocapsids. Staining of microtubules and the nucleus is the same as that described in the legend to panel A.

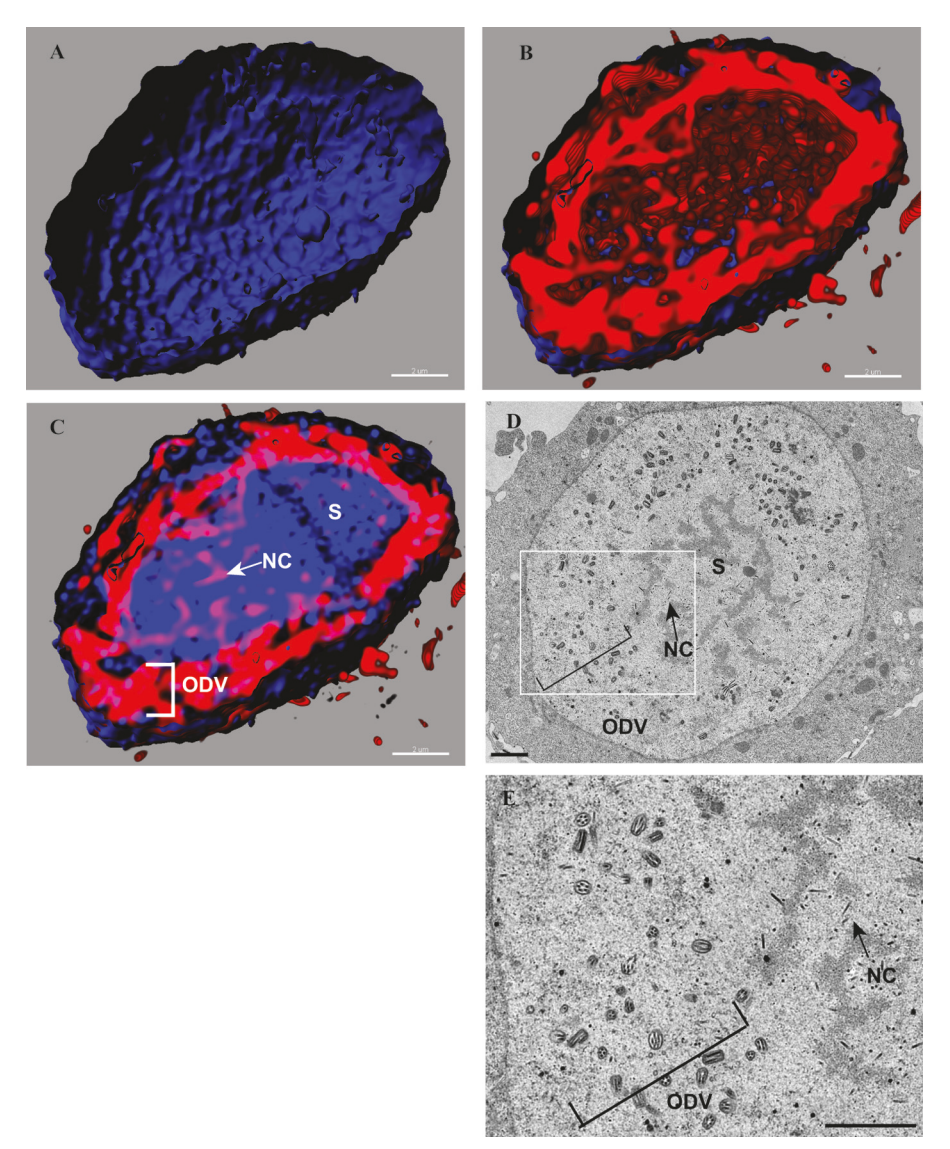


FIG 10 Analysis of the nucleus of Tn5B1 cells infected with VP39-3×mCherry. (A to C) Cross sections through a three-dimensional rendering of the nucleus of a representative Tn5B1 cell infected with VP39-3×mCherry. (A) Surface rendering of the outside of the DAPI-stained nucleus. (B) Surface rendering of regions of VP39-3×mCherry within the nucleus. (C) Merged image of panels A and B plus the central virogenic stroma (lighter blue) also stained by DAPI. Note the regions of VP39-3×mCherry infiltrating the virogenic stroma (S) and the dense regions surrounding the stroma. The images in panels A to C were generated using Imaris software. (D) Cross section of an electron micrograph of a Tn5B1 cell infected with WT virus showing the equivalent regions shown in panel C, including the virogenic stroma, the regions of single nucleocapsid assembly within the stromal spaces (NC), and the regions of ODV assembly surrounding the virogenic stroma. (E) Enlarged region of the area shown by the white box in panel D. Bars = 2  $\mu$ m.

AcMNPV nucleocapsid proteins with *T. ni* kinesin-1 and microtubules and that kinesin-1 is required for BV production.

To analyze the interaction of nucleocapsid or nucleocapsid proteins with *T. ni* kinesin-1 and its component proteins, KLC and KHC, a multifaceted approach was taken. This included cloning of the *T. ni* KLC and KHC genes, coimmunoprecipitation analysis, colocalization by fluorescence microscopy, siRNA inhibition, and yeast two-hybrid analysis. We showed that HA-AC141 specifically coimmunoprecipitates host *T. ni* KLC (Fig. 1).

In reciprocal pulldown experiments, we found that WT virus AC141 specifically pulled down N- or C-HA-KLC by coimmuno-precipitation. Conversely, each of the tagged kinesin-1 molecules, i.e., HA-tagged KLC and KHC, specifically pulled down WT virus

AC141 (Fig. 3). AC141 is a nucleocapsid-associated protein, but it is also present throughout the cytoplasm and is concentrated toward the cellular periphery regions (5). Therefore, to determine if coimmunoprecipitation was pulling down nucleocapsids, immunoprecipitated complexes were analyzed for the presence of other nucleocapsid proteins. We found that the major capsid protein VP39, as well as the capsid-associated proteins BV/ODV-C42 and FP25, was specifically coimmunoprecipitated with HA-tagged KLC (Fig. 8). Thus, these results support the conclusion that AcMNPV nucleocapsids associate with *T. ni* kinesin-1.

The association of AC141 with KLC and KHC was further analyzed by confocal microscopy, and it was observed that HA-AC141 colocalized with Myc-tagged KLC and KHC mainly in the

TABLE 2 Yeast two-hybrid screening for direct interaction of KHC and KLC with AC141 or VP39

		Growth of colonies on <sup>d</sup> :	
pBD construct	pAD construct	Leu- and Trp-deficient medium	Leu-, Trp-, and His-deficient medium
Empty	Empty <sup>a</sup>	+	_
KHC	$KLC^b$	+	+
KLC	$Empty^c$	+	+
KHC	Empty	_	_
KLC	AC141	+	+
TPR	AC141	+	_
$\Delta$ AC141	KLC	+	_
$\Delta$ AC141	TPR	+	_
KLC	VP39	+	+
TPR	VP39	+	_
VP39	KLC	+	_
VP39	TPR	+	_
KHC	AC141	+	_
Stalk/tail	AC141	+	_
$\Delta$ AC141	KHC	+	_
$\Delta$ AC141	Stalk/tail	+	_
KHC	VP39	+	_
Stalk/tail	VP39	+	_
VP39	KHC	+	_
VP39	Stalk/tail	+	_

<sup>&</sup>lt;sup>a</sup> Negative control.

cellular periphery regions near the plasma membrane (Fig. 4 and 5). Analysis within these colocalized regions showed high Pearson's overlap coefficients, indicating that there is a significant synchrony in intensity in areas of overlap and therefore strongly suggesting a functional colocalization. We further confirmed that at the cellular periphery, the regions of colocalization between AC141 and KLC or KHC also colocalize with  $\beta$ -tubulin (Fig. 6).

It was previously shown using fluorescence microscopy that a virus expressing the VP39 capsid protein fused to the fluorescent protein mCherry (VP39-3×mCherry) could be used to detect individual nucleocapsids interacting with actin filaments during virus entry (11). In this study, we used the VP39-3×mCherry construct to examine the association of the nucleocapsid with microtubules during entry and egress (Fig. 9). The results indicated that during entry and transport by actin, the colocalization of nucleocapsids with microtubules was very limited, as expected. However, during egress, the majority of nucleocapsids colocalized with microtubules. This result further supports the conclusion that kinesin-1 is involved in the transport of nucleocapsids along microtubules during egress.

VP39-3×mCherry was present at a high level in the nucleus at late times postinfection (Fig. 9C). Intriguingly, the distribution in the nucleus showed distinct filamentous band structures permeating and surrounding the virogenic stroma, suggesting that the distinct sites of nucleocapsid and ODV assembly are separate from the site of viral DNA replication (Fig. 10). Compared with the extremely high levels of VP39-3×mCherry observed in the nucleus (where nucleocapsid assembly occurs), the levels of VP39-3×mCherry associated with individual nucleocapsids in the cytoplasm appeared to be much lower, as expected.

The results of the coimmunoprecipitation and colocalization studies described here, in combination with previously published data (17, 18), suggest that nucleocapsids are transported by kinesin-1 on microtubules, prior to the final assembly and budding of BV at the plasma membrane. We further tested this model by performing siRNA experiments in which kinesin-1 was downregulated. If kinesin-1 is involved in nucleocapsid transport to the plasma membrane, the downregulation of kinesin-1 should reduce the level of production of BV. Our results showed a clear reduction of the level of BV production under these conditions (Fig. 7C). Similar strategies involving siRNA downregulation of KLC or the use of a dominant negative mutant of KLC have been used to show kinesin-1 KLC involvement in virion transport and processing of ASFV and adenovirus (30, 39). The current experiments represent the first direct demonstration of the importance of microtubule motor proteins in the production of baculovirus BV.

Danquah et al. (18) determined by FRET-FILM analysis with the *D. melanogaster* KLC TPR motif that AC141 and VP39 but not ORF1629 directly interact. The results of our coimmunoprecipitation, colocalization, and siRNA assays using KLC and KHC from the natural host T. ni are consistent with these previous results and provide substantial evidence that these interactions are relevant in the naturally infected host. It is also of interest that in a yeast two-hybrid analysis, AC141 and VP39 failed to show any direct interactions with KLC and KHC (Table 2). It is possible that AC141 or VP39 needs to be associated with the exported nucleocapsid to interact with kinesin-1, which would account for the negative result in the yeast two-hybrid analysis. Alternatively, other nucleocapsid proteins, nucleocapsid-associated proteins (3), or cellular cargo adaptor proteins (19) may be required for the direct interaction with kinesin-1. If AC141 or VP39 binds a cellular adaptor protein which binds the TPR motif, that could explain the previous FRET-FLIM results (18). Specific viral proteins that directly bind kinesin-1 have been identified in vaccinia virus (A36R) and HSV-1 (US11), both of which utilize microtubules for anterograde transport (27, 33). Both US11 and A36R were shown to bind directly to KHC and KLC, respectively, as bacterially expressed proteins or by yeast two-hybrid analysis. The results of this study show that kinesin-1 is involved in BV production and that AcMNPV nucleocapsid proteins are found in a complex with kinesin-1. However, it remains to be determined which viral protein directly mediates this interaction.

In conclusion, the cumulative data from this and prior studies indicate that anterograde transport of AcMNPV nucleocapsids utilizes the microtubule transport system. Because in this virus viral entry is mediated by actin polymerization for retrograde transport (11-13), it is interesting that the virus takes advantage of two quite separate systems for trafficking nucleocapsids through the cytosol to and from the nucleus. This difference in trafficking is perhaps not surprising, as AcMNPV also uses quite disparate mechanisms to enter and exit the nucleus. While incoming AcMNPV nucleocapsids interact with and are transported through nuclear pores (55), newly synthesized progeny nucleocapsids exit the nucleus not through the nuclear pore but by budding through the nuclear envelope (2, 16). Indeed, enveloped nucleocapsids have been observed by electron microscopy (EM) in the cytoplasm of infected cells (16), and these envelopes are presumably derived from the nuclear membrane(s). On the basis of EM data, it was also speculated that these envelopes were rapidly

<sup>&</sup>lt;sup>b</sup> Positive control.

<sup>&</sup>lt;sup>c</sup> Autotransactivation.

d+, growth; -, no growth.

lost (16). It is possible that microtubules are involved in transporting both the enveloped and the nonenveloped nucleocapsids upon exit from the nucleus. Microtubule transport has a distinct advantage over actin transport due to its well-characterized directionality (34, 35). However, it is clear that additional studies will be necessary before we can fully understand the complex interactions that regulate and mediate nucleocapsid trafficking during viral entry and egress.

#### **ACKNOWLEDGMENTS**

This study was supported in part by funding from the Natural Science and Engineering Research Council (to D.A.T.) and NSF project 1354421 (to G.W.B.).

We thank Matthew D. Welch and Taro Ohkawa for kindly providing the VP39-3×mCherry construct. We also thank Leslie G. Willis for excellent technical assistance and experimental suggestions and Michael Weis for his expertise with confocal microscopy.

### **FUNDING INFORMATION**

National Science Foundation (NSF) provided funding to Gary W. Blissard under grant number 1354421. Gouvernement du Canada | Natural Sciences and Engineering Research Council of Canada (NSERC) provided funding to David A. Theilmann.

#### **REFERENCES**

- Braunagel SC, Summers MD. 2007. Molecular biology of the baculovirus occlusion-derived virus envelope. Curr Drug Targets 8:1084–1095. http://dx.doi.org/10.2174/138945007782151315.
- Rohrmann GF. 2013. Baculovirus molecular biology, 3rd ed. National Center for Biotechnology Information, Bethesda, MD.
- Wang R, Deng F, Hou D, Zhao Y, Guo L, Wang H, Hu Z. 2010. Proteomics of the *Autographa californica* nucleopolyhedrovirus budded virions. J Virol 84:7233–7242. http://dx.doi.org/10.1128/JVI.00040-10.
- Dai X, Stewart TM, Pathakamuri JA, Li Q, Theilmann DA. 2004. Autographa californica multiple nucleopolyhedrovirus exon0 (orf141), which encodes a RING finger protein, is required for efficient production of budded virus. J Virol 78:9633–9644. http://dx.doi.org/10.1128/JVI.78 .18.9633-9644.2004.
- Fang M, Dai X, Theilmann DA. 2007. Autographa californica multiple nucleopolyhedrovirus EXON0 (ORF141) is required for efficient egress of nucleocapsids from the nucleus. J Virol 81:9859–9869. http://dx.doi.org /10.1128/JVI.00588-07.
- Fang M, Nie Y, Dai X, Theilmann DA. 2008. Identification of AcMNPV EXON0 (ac141) domains required for efficient production of budded virus, dimerization and association with BV/ODV-C42 and FP25. Virology 375:265–276. http://dx.doi.org/10.1016/j.virol.2008.01.036.
- Monsma SA, Oomens AG, Blissard GW. 1996. The GP64 envelope fusion protein is an essential baculovirus protein required for cell-to-cell transmission of infection. J Virol 70:4607–4616.
- 8. Oomens AG, Blissard GW. 1999. Requirement for GP64 to drive efficient budding of *Autographa californica* multicapsid nucleopolyhedrovirus. Virology 254:297–314. http://dx.doi.org/10.1006/viro.1998.9523.
- Charlton CA, Volkman LE. 1993. Penetration of Autographa californica nuclear polyhedrosis virus nucleocapsids into IPLB Sf 21 cells induces actin cable formation. Virology 197:245–254. http://dx.doi.org/10.1006/viro.1993.1585.
- Lanier LM, Volkman LE. 1998. Actin binding and nucleation by Autographa californica M nucleopolyhedrovirus. Virology 243:167–177. http://dx.doi.org/10.1006/viro.1998.9065.
- 11. Ohkawa T, Volkman LE, Welch MD. 2010. Actin-based motility drives baculovirus transit to the nucleus and cell surface. J Cell Biol 190:187–195. http://dx.doi.org/10.1083/jcb.201001162.
- Mueller J, Pfanzelter J, Winkler C, Narita A, Le Clainche C, Nemethova M, Carlier MF, Maeda Y, Welch MD, Ohkawa T, Schmeiser C, Resch GP, Small JV. 2014. Electron tomography and simulation of baculovirus actin comet tails support a tethered filament model of pathogen propulsion. PLoS Biol 12:e1001765. http://dx.doi.org/10.1371/journal.pbio .1001765.
- 13. Ohkawa T, Volkman LE. 1999. Nuclear F-actin is required for AcMNPV

- nucleocapsid morphogenesis. Virology 264:1–4. http://dx.doi.org/10.1006/viro.1999.0008.
- Goley ED, Ohkawa T, Mancuso J, Woodruff JB, D'Alessio JA, Cande WZ, Volkman LE, Welch MD. 2006. Dynamic nuclear actin assembly by Arp2/3 complex and a baculovirus WASP-like protein. Science 314:464–467. http://dx.doi.org/10.1126/science.1133348.
- 15. Marek M, Merten OW, Galibert L, Vlak JM, van Oers MM. 2011. Baculovirus VP80 protein and the F-actin cytoskeleton interact and connect the viral replication factory with the nuclear periphery. J Virol 85: 5350–5362. http://dx.doi.org/10.1128/JVI.00035-11.
- Granados RR, Lawler KA. 1981. In vivo pathway of Autographa californica baculovirus invasion and infection. Virology 108:297–308. http://dx .doi.org/10.1016/0042-6822(81)90438-4.
- Fang M, Nie Y, Theilmann DA. 2009. AcMNPV EXON0 (AC141) which
  is required for the efficient egress of budded virus nucleocapsids interacts
  with β-tubulin. Virology 385:496–504. http://dx.doi.org/10.1016/j.virol
  .2008.12.023.
- Danquah JO, Botchway S, Jeshtadi A, King LA. 2012. Direct interaction of baculovirus capsid proteins VP39 and EXON0 with kinesin-1 in insect cells determined by fluorescence resonance energy transfer-fluorescence lifetime imaging microscopy. J Virol 86:844–853. http://dx.doi.org/10 .1128/JVI.06109-11.
- 19. Hirokawa N, Noda Y, Tanaka Y, Niwa S. 2009. Kinesin superfamily motor proteins and intracellular transport. Nat Rev Mol Cell Biol 10:682–696. http://dx.doi.org/10.1038/nrm2774.
- Schnapp BJ. 2003. Trafficking of signaling modules by kinesin motors. J Cell Sci 116:2125–2135. http://dx.doi.org/10.1242/jcs.00488.
- Gauger AK, Goldstein LS. 1993. The *Drosophila* kinesin light chain. Primary structure and interaction with kinesin heavy chain. J Biol Chem 268:13657–13666.
- 22. Gindhart JG, Jr, Goldstein LS. 1996. Tetratrico peptide repeats are present in the kinesin light chain. Trends Biochem Sci 21:52–53. http://dx.doi.org/10.1016/S0968-0004(96)80180-0.
- Hirokawa N, Takemura R. 2005. Molecular motors and mechanisms of directional transport in neurons. Nat Rev Neurosci 6:201–214. http://dx .doi.org/10.1038/nrn1624.
- Adio S, Reth J, Bathe F, Woehlke G. 2006. Review: regulation mechanisms of kinesin-1. J Muscle Res Cell Motil 27:153–160. http://dx.doi.org/10.1007/s10974-005-9054-1.
- 25. Ward BM, Moss B. 2001. Vaccinia virus intracellular movement is associated with microtubules and independent of actin tails. J Virol 75:11651–11663. http://dx.doi.org/10.1128/JVI.75.23.11651-11663.2001.
- Hollinshead M, Rodger G, Van Eijl H, Law M, Hollinshead R, Vaux DJ, Smith GL. 2001. Vaccinia virus utilizes microtubules for movement to the cell surface. J Cell Biol 154:389–402. http://dx.doi.org/10.1083/jcb .200104124.
- Ward BM, Moss B. 2004. Vaccinia virus A36R membrane protein provides a direct link between intracellular enveloped virions and the microtubule motor kinesin. J Virol 78:2486–2493. http://dx.doi.org/10.1128/JVI.78.5.2486-2493.2004.
- 28. Morgan GW, Hollinshead M, Ferguson BJ, Murphy BJ, Carpentier DC, Smith GL. 2010. Vaccinia protein F12 has structural similarity to kinesin light chain and contains a motor binding motif required for virion export. PLoS Pathog 6:e1000785. http://dx.doi.org/10.1371/journal.ppat.1000785.
- 29. Carpentier DC, Gao WN, Ewles H, Morgan GW, Smith GL. 2015. Vaccinia virus protein complex F12/E2 interacts with kinesin light chain isoform 2 to engage the kinesin-1 motor complex. PLoS Pathog 11: e1004723. http://dx.doi.org/10.1371/journal.ppat.1004723.
- 30. Jouvenet N, Monaghan P, Way M, Wileman T. 2004. Transport of African swine fever virus from assembly sites to the plasma membrane is dependent on microtubules and conventional kinesin. J Virol 78:7990–8001. http://dx.doi.org/10.1128/JVI.78.15.7990-8001.2004.
- de Matos AP, Carvalho ZG. 1993. African swine fever virus interaction with microtubules. Biol Cell 78:229–234. http://dx.doi.org/10.1016/0248 -4900(93)90134-Z.
- 32. Radtke K, Kieneke D, Wolfstein A, Michael K, Steffen W, Scholz T, Karger A, Sodeik B. 2010. Plus- and minus-end directed microtubule motors bind simultaneously to herpes simplex virus capsids using different inner tegument structures. PLoS Pathog 6:e1000991. http://dx.doi.org/10.1371/journal.ppat.1000991.
- 33. Diefenbach RJ, Miranda-Saksena M, Diefenbach E, Holland DJ, Boadle RA, Armati PJ, Cunningham AL. 2002. Herpes simplex virus tegument

- protein US11 interacts with conventional kinesin heavy chain. J Virol 76:3282–3291. http://dx.doi.org/10.1128/JVI.76.7.3282-3291.2002.
- Dohner K, Nagel CH, Sodeik B. 2005. Viral stop-and-go along microtubules: taking a ride with dynein and kinesins. Trends Microbiol 13:320–327. http://dx.doi.org/10.1016/j.tim.2005.05.010.
- 35. Greber UF, Way M. 2006. A superhighway to virus infection. Cell 124: 741–754. http://dx.doi.org/10.1016/j.cell.2006.02.018.
- Dodding MP, Way M. 2011. Coupling viruses to dynein and kinesin-1. EMBO J 30:3527–3539. http://dx.doi.org/10.1038/emboj.2011.283.
- 37. Ward BM. 2011. The taking of the cytoskeleton one two three: how viruses utilize the cytoskeleton during egress. Virology 411:244–250. http://dx.doi.org/10.1016/j.virol.2010.12.024.
- Diefenbach RJ, Miranda-Saksena M, Douglas MW, Cunningham AL. 2008. Transport and egress of herpes simplex virus in neurons. Rev Med Virol 18:35–51. http://dx.doi.org/10.1002/rmv.560.
- Strunze S, Engelke MF, Wang IH, Puntener D, Boucke K, Schleich S, Way M, Schoenenberger P, Burckhardt CJ, Greber UF. 2011. Kinesin-1-mediated capsid disassembly and disruption of the nuclear pore complex promote virus infection. Cell Host Microbe 10:210–223. http://dx.doi.org/10.1016/j.chom.2011.08.010.
- Lukic Z, Dharan A, Fricke T, Diaz-Griffero F, Campbell EM. 2014. HIV-1 uncoating is facilitated by dynein and kinesin 1. J Virol 88:13613–13625. http://dx.doi.org/10.1128/JVI.02219-14.
- 41. Luckow VA, Lee SC, Barry GF, Olins PO. 1993. Efficient generation of infectious recombinant baculoviruses by site-specific transposon-mediated insertion of foreign genes into a baculovirus genome propagated in *Escherichia coli*. J Virol 67:4566–4579.
- Chen YR, Zhong S, Fei Z, Gao S, Zhang S, Li Z, Wang P, Blissard GW. 2014. Transcriptome responses of the host *Trichoplusia ni* to infection by the baculovirus *Autographa californica* multiple nucleopolyhedrovirus. J Virol 88:13781–13797. http://dx.doi.org/10.1128/JVI.02243-14.
- 43. Pfeifer TA, Guarna MM, Kwan EM, Lesnicki G, Theilmann DA, Grigliatti TA, Kilburn DG. 2001. Expression analysis of a modified factor X in stably transformed insect cell lines. Protein Expr Purif 23:233–241. http://dx.doi.org/10.1006/prep.2001.1503.
- 44. Pfeifer TA, Hegedus DD, Grigliatti TA, Theilmann DA. 1997. Baculovirus immediate-early promoter-mediated expression of the zeocin resistance gene for use as a dominant selectable marker in dipteran and lepidopteran insect cell lines. Gene 188:183–190. http://dx.doi.org/10.1016/S0378-1119(96)00756-1.

- Yang P, Sampson HM, Krause HM. 2006. A modified tandem affinity purification strategy identifies cofactors of the Drosophila nuclear receptor dHNF4. Proteomics 6:927–935. http://dx.doi.org/10.1002/pmic .200500230.
- Carpentier DCJ, Griffiths CM, King LA. 2008. The baculovirus P10 protein of *Autographa californica* nucleopolyhedrovirus forms two distinct cytoskeletal-like structures and associates with polyhedral occlusion bodies during infection. Virology 371:278–291. http://dx.doi.org/10.1016/j.virol.2007.09.043.
- 47. Braunagel SC, Burks JK, Rosas-Acosta G, Harrison RL, Ma H, Summers MD. 1999. Mutations within the *Autographa californica* nucleopolyhedrovirus FP25K gene decrease the accumulation of ODV-E66 and alter its intranuclear transport. J Virol 73:8559–8570.
- Braunagel SC, Guidry PA, Rosas-Acosta G, Engelking L, Summers MD. 2001. Identification of BV/ODV-C42, an *Autographa californica* nucleopolyhedrovirus orf101-encoded structural protein detected in infectedcell complexes with ODV-EC27 and p78/83. J Virol 75:12331–12338. http: //dx.doi.org/10.1128/IVL75.24.12331-12338.2001.
- 49. Campbell MJ. 1995. Lipofection reagents prepared by a simple ethanol injection technique. Biotechniques 18:1027–1032.
- Reed LJ, Muench H. 1938. A simple method of estimating fifty per cent endpoints. Am J Epidemiol 27:493–497.
- 51. Volkman LE, Zaal KJ. 1990. *Autographa californica* M nuclear polyhedrosis virus: microtubules and replication. Virology 175:292–302. http://dx.doi.org/10.1016/0042-6822(90)90211-9.
- Manji GA, Friesen PD. 2001. Apoptosis in motion. An apical, P35insensitive caspase mediates programmed cell death in insect cells. J Biol Chem 276:16704–16710.
- 53. Mu J, van Lent JW, Smagghe G, Wang Y, Chen X, Vlak JM, van Oers MM. 2014. Live imaging of baculovirus infection of midgut epithelium cells: a functional assay of per os infectivity factors. J Gen Virol 95:2531–2539. http://dx.doi.org/10.1099/vir.0.068262-0.
- 54. Wang Q, Liang C, Song J, Chen X. 2007. HA2 from the *Helicoverpa armigera* nucleopolyhedrovirus: a WASP-related protein that activates Arp2/3-induced actin filament formation. Virus Res 127:81–87. http://dx.doi.org/10.1016/j.virusres.2007.03.021.
- 55. Au S, Wu W, Pante N. 2013. Baculovirus nuclear import: open, nuclear pore complex (NPC) sesame. Viruses 5:1885–1900. http://dx.doi.org/10.3390/v5071885.